

Acetylcholinesterase: Enzyme Structure, Reaction Dynamics, and Virtual Transition States

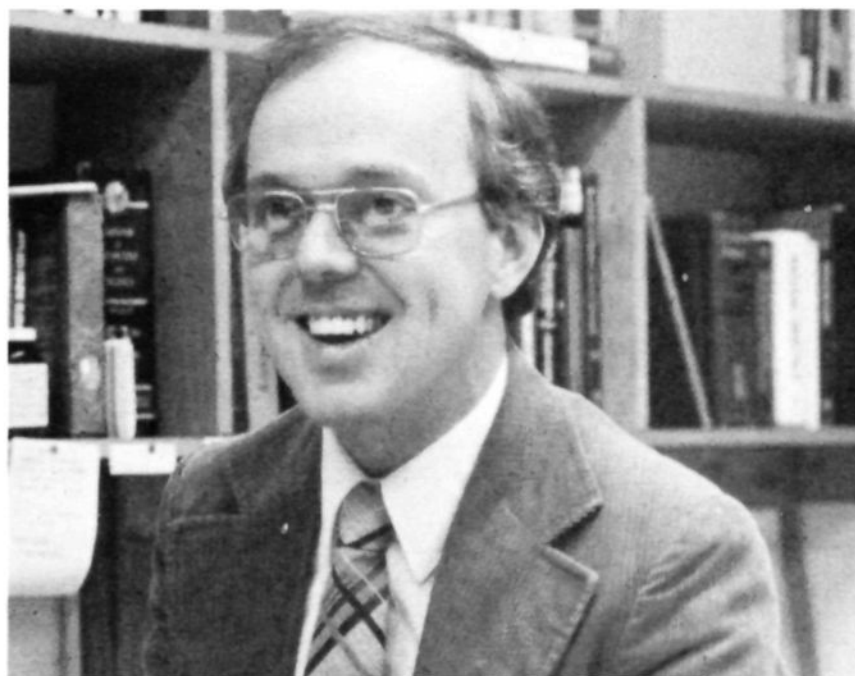
DANIEL M. QUINN

Department of Chemistry, The University of Iowa, Iowa City, Iowa 52242

Received February 5, 1987 (Revised Manuscript Received May 28, 1987)

Contents

I. Introduction	955
A. Physiological Function and Biomedical Significance	955
B. General Catalytic Mechanism	957
C. AChE Catalytic Power	957
II. AChE Structure	958
A. Tertiary and Quaternary Structure	958
B. Primary Structure	959
C. Active Site Structure	960
1. Esteratic Locus	960
2. Anionic Locus	961
3. Hydrophobic Regions	965
III. Reaction Dynamics	965
A. Introduction	965
B. The Virtual Transition-State Concept	966
1. Reaction Thermodynamics and Free Energy Diagrams	966
2. Kinetic Equations	966
3. Kinetic Solvent Isotope Effects: Predictions	967
4. pH-Rate Profiles	969
C. Virtual Transition States for Anilide Hydrolyses	969
1. Probes of Virtual Transition States for k_E	969
2. Consideration of Alternate Models	972
3. Solvent Isotope Effects and Effective (Virtual) Reactant State for k_{ES}	973
4. Free Energy Diagram for Anilide Hydrolyses	974
D. Virtual Transition States for Ester Hydrolyses	974
1. Probes of Virtual Transition States for k_E	974
2. Probes of Virtual Transition States for k_{ES}	975
3. Free Energy Diagram for Ester Hydrolyses	976
E. Structural Features of Chemical Transition States	976
IV. AChE Reaction Dynamics and the Evolution of Enzyme Catalytic Power	977
V. Future Directions	977
VI. References and Notes	978



Daniel M. Quinn was born in Monroe City, MO, on January 30, 1950. He received a B.S. in chemistry in 1972 from Quincy College, Quincy, IL. His graduate work in physical organic chemistry under Richard L. Schowen of the University of Kansas Chemistry Department culminated in a Ph.D. degree in 1977. Two postdoctoral appointments followed: the first, with Eugene H. Cordes of the Indiana University Chemistry Department (1978-1980), involved characterization of molecular dynamics and phase organization of lipids and lipoproteins by ^{13}C NMR; the second was an NIH Traineeship in the laboratory of Judith A. K. Harmony of the University of Cincinnati College of Medicine, and it introduced Dr. Quinn to the vagaries of lipoprotein lipase catalysis. Dr. Quinn moved to the University of Iowa Department of Chemistry in 1982 as an Assistant Professor and was elevated to Associate Professor in 1987. His current research interests are characterization of reaction dynamics of hydrolytic enzymes (lipoprotein lipase, cholesterol esterase, and cholinesterases) by isotope effects and other kinetics measurements and the design of mechanism-based enzyme effectors. Dr. Quinn was elected Fellow of the Council on Arteriosclerosis of the American Heart Association in 1982. He has received a New Investigator Research Award (1982-1985) and a Research Career Development Award (1985-1990) from the National Heart, Lung and Blood Institute of the National Institutes of Health.

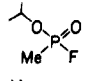
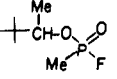
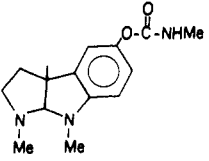
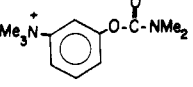
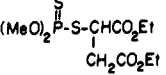
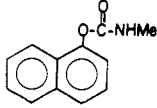
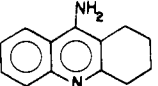
central and peripheral nervous systems, along with the acetylcholine (ACh) receptor, in the transmission of action potentials across nerve-nerve and neuromuscular synapses.² The enzyme's physiological task is the hydrolytic destruction of the cationic neurotransmitter ACh. AChE is an extrinsic membrane-bound enzyme that projects into the synapse. The enzyme springs into action when ACh is released from the presynaptic nerve process in response to an action potential. ACh diffuses across the synapse and binds to the ACh receptor, which among other functions serves as an ion gate for the entry of K^+ into the postsynaptic nerve process or muscle cell. A series of events follows that results in triggering the action potential in the postsynaptic cell. AChE rapidly terminates the ACh receptor-mediated

I. Introduction

A. Physiological Function and Biomedical Significance

Acetylcholinesterase (acetylcholine acetylhydrolase, EC 3.1.1.7; abbreviated herein AChE¹) functions in the

CHART I. Some Inhibitors of AChE

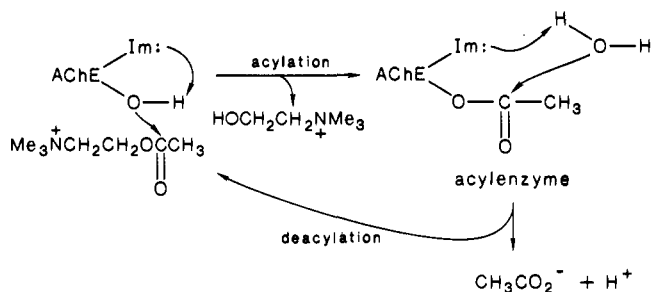
structure	name	comments	ref
	isopropyl methylphosphonofluoridate (sarin)	chemical warfare agent; very toxic "nerve gas"	3
	pinacolyl methylphosphonofluoridate (soman)	chemical warfare agent; very toxic "nerve gas"	3
	physostigmine	salicylate salt used to treat acute congestive glaucoma	3
	neostigmine	used to treat myasthenia gravis	3
	malathion	insecticide; used to combat the medfly	3
	carbaril	insecticide; component of sevin bug dust	3
	1,2,3,4-tetrahydro-9-aminoacridine (THA)	used in clinical trials to allay symptoms of Alzheimer's disease	4

ion gating by hydrolyzing ACh.²

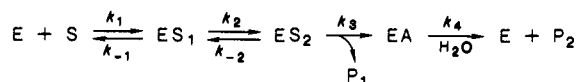
Because of the pivotal role that AChE plays in the nervous system, the enzyme has long been an attractive target for the rational design of mechanism-based inhibitors. A sampling of AChE inhibitors is shown in Chart I. These compounds illustrate the range of effects that AChE inhibitors manifest. For example, the chemical warfare agents sarin and soman rapidly phosphorylate a serine residue in the enzyme's active site.³ These compounds are among the most toxic agents ever synthesized by humans and kill by inducing circulatory and respiratory failure via AChE inhibition in the peripheral nervous system. In contrast, the carbamates physostigmine and neostigmine are useful therapeutic agents in the treatment of glaucoma and myasthenia gravis, respectively.³ The mechanism by which these carbamates manifest their biomedical effects likely involves transient carbamylation of the active site serine of AChE. A recent report supports a guarded optimism that reversible inhibitors of AChE that can make their way into the central nervous system may be useful in allaying the symptoms of Alzheimer's disease.³⁻⁵ A hallmark of the disease is a developing cholinergic deficit as the disease progresses.⁶ Thus, it may be possible to increase ACh levels in affected regions of the brain by inhibiting AChE. Accordingly, 1,2,3,4-tetrahydro-9-aminoacridine significantly improved the memories of 16 of 17 elderly Alzheimer's patients in a clinical trial.⁴ The insecticide malathion was instrumental in combating the medfly infestation in the U.S. in the early 1980s. The species specificity of this AChE inhibitor gives rise to its low toxicity in man and its consequent usefulness in ridding the human food chain of the medfly. As the examples discussed in this paragraph and in Chart I emphasize, our society has a considerable economic, medical, and national security interest in AChE catalysis.

The purpose of this review is not, however, to detail the encyclopedic efforts that have gone into the development and evaluation of AChE inhibitors. Despite the voluminous nature of the AChE literature, the AChE mechanism remains an enigma. This enigma has its basis in both human nature and in evolution. Scientists (human nature) have been quick to consider AChE catalysis an open-and-shut case. As we shall see, wishful analogy between AChE catalysis and the reasonably well-characterized action of serine proteases⁷⁻⁹ is partly responsible for this. Evolution's contribution to the AChE enigma derives from the fact that the catalytic power of the enzyme is so highly developed that, at least under some experimental conditions, chemically uninteresting microscopic events are rate limiting. This review will explore work of the past several years on the structure and reaction dynamics of AChE that dispel the myth of strict serine protease analogy. Experiments will be discussed that are beginning to penetrate the enigma of AChE catalysis by providing information on the microscopic events that contribute to rate determination and on the structural features of the chemical transition states that serve as the focus for the evolution of the enzyme's catalytic power. In detailing these experiments, the virtual transition-state approach to describing complex enzyme reaction dynamics will be developed. The virtual transition-state concept¹⁰⁻¹² was first described by Schowen¹⁰ in 1978 and in the intervening years has been used to characterize reaction dynamics and transition-state structures for serine protease¹³⁻¹⁷ and AChE¹⁸⁻²² reactions. As will be shown below (III. Reaction Dynamics B. The Virtual Transition-State Concept) for the AChE mechanism, the virtual transition-state approach is equivalent to the approach introduced by Northrop^{23,24} for probing reaction dynamics and transition-state structures of enzyme-catalyzed reactions.

SCHEME I. Acylenzyme Mechanism for AChE Catalysis



SCHEME II. Kinetic Mechanism for AChE Catalysis that Incorporates an Induced-Fit Step



E = AChE, S = substrate, EA = acylenzyme, P_1, P_2 = products.
 ES_1 = Michaelis complex, ES_2 = induced-fit complex

B. General Catalytic Mechanism

AChE catalysis occurs via an acylenzyme mechanism that involves nucleophilic (serine) and general acid-base (histidine) elements,^{2,25} as outlined in Scheme I. Froede and Wilson²⁶ recently provided the first direct evidence for the Scheme I mechanism by trapping the acylenzyme generated during AChE-catalyzed turnover of ACh and acetylthiocholine (ATCh) at $[S]_0 \gg K_m$. For the ACh and ATCh reactions 68% and 57%, respectively, of the enzyme was in the acylenzyme form. These results show that acylation and deacylation both contribute to rate limitation when V_{max} is measured. Though the Scheme I mechanism is similar pro forma to that of serine proteases,⁷⁻⁹ there are numerous features of AChE catalysis that are distinct. These features will be discussed at various points in this review.

Terrone Rosenberry^{2,27} suggested that at least for neutral ester substrates an induced-fit conformation change of AChE occurs after substrate binding but before chemical catalysis. Accordingly, the minimal kinetic mechanism is that of Scheme II. In this mechanism, k_3 and k_4 are the chemical steps for acylation and deacylation, respectively. The steady-state kinetic parameters for the mechanism of Scheme II are given in eq 1 and 2. The steady-state rate constants

$$k_{ES} = \frac{k_2 k_3 k_4}{k_2 k_3 + k_4(k_2 + k_{-2} + k_3)} \quad (1)$$

$$k_E = \frac{k_1 k_2 k_3}{k_{-1}(k_{-2} + k_3) + k_2 k_3} \quad (2)$$

are defined as k_{ES} and k_E to emphasize the initial states to which the rate constants refer, i.e., bound states and free enzyme, respectively. As eq 2 shows, k_E monitors conversion of free enzyme and free substrate to a transition state(s) in the acylation stage of catalysis. The rate constant k_{ES} monitors conversion of bound states (ES_1 and/or ES_2 and/or EA) to transition states for acylation and/or deacylation. Hence, k_E always probes acylation reaction dynamics, whereas k_{ES} probes acylation and/or deacylation.

Rosenberry based his assignment of AChE reaction dynamics on the following observations: (1) pK_a values determined from pH- k_E profiles are well below the intrinsic $pK_a \sim 6.3$ of the active site histidine^{2,25,27} for

reactive neutral ester substrates, such as phenyl acetate and isoamyl acetate. (2) pK_a values for k_E of the less reactive ester *p*-nitrophenyl acetate and for inhibition of the enzyme by diethyl *p*-nitrophenyl phosphate are 6.1 and 6.2, respectively, and thus more closely approximate the intrinsic pK_a . (3) Solvent isotope effects for k_E of reactive neutral esters are near unity, while those for k_E of less reactive esters and for k_{ES} of all substrates are ~ 2 . Rosenberry suggested that low solvent isotope effects and pK_a values for k_E arise because acylation²⁸ is prominently rate limited by the pH-insensitive and solvent isotope-insensitive k_2 step.

Equation 2 can be used to rationalize Rosenberry's observations. For example, modest rearranging of eq 2 gives eq 3. In eq 3, $k_3' = k_1 k_2 k_3 / k_{-1} k_{-2}$ is the overall

$$k_E = k_3' / (1 + C), \text{ where } C = k_3 / k_{-2,1} \quad (3)$$

rate constant for conversion of E + S to the transition state of the k_3 step (i.e., the chemical acylation transition state). The rate constant $k_{-2,1}$ is a composite rate constant²⁹ for reversion of ES_2 to E + S, and comes from eq 4. C in eq 3 is the commitment to chemical

$$1/k_{-2,1} = 1/k_{-2} + k_2/k_{-1}k_{-2} \quad (4)$$

catalysis in the acylation stage of the AChE reaction and measures the tendency of ES_2 to proceed to the acylenzyme EA vs. reversion to E + S. When C is small $k_E = k_3'$ and the pH-sensitive and solvent isotope-sensitive chemical transition state is solely rate determining. However, when C is large k_E is given by eq 5. In

$$k_E = \frac{k_1 k_2}{k_{-1} + k_2} \quad (5)$$

this case, k_1 and/or k_2 is rate determining. Since these rate constants are for substrate binding and induced fit, respectively, it is not surprising that they would not be pH sensitive or produce solvent isotope effects. The low pK_a values and solvent isotope effects reported by Rosenberry²⁷ for good neutral ester substrates of AChE thus have their origins in prominent rate determination by k_1 and/or k_2 .

Though Rosenberry's account of acylation reaction dynamics is intuitively satisfying, it lacks a quantitative basis. Unanswered questions remain: (1) To what extent do chemical and nonchemical events contribute to rate determination? (2) What are the structural features of the transition state of the chemical step k_3 ? (3) What is the intrinsic pK_a on which the k_3 step depends? Approaches to answering these questions will be outlined in the section on reaction dynamics that deals with the virtual transition-state concept. Moreover, results for AChE-catalyzed hydrolysis of neutral esters and anilides will be detailed.

C. AChE Catalytic Power

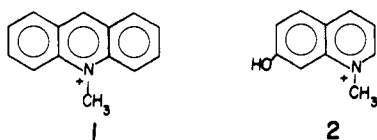
One fact stands out concerning AChE catalysis: the enzyme has amazing catalytic power. The turnover number k_{ES} is $>10^4 \text{ s}^{-1}$,² which is among the highest turnover numbers reported for enzyme catalysis. For the physiological substrate ACh k_E is $>10^8 \text{ M}^{-1} \text{ s}^{-1}$,^{2,30} and therefore, diffusion of ACh to the active site is probably rate determining.³¹ This high second-order rate constant is a hallmark of an evolutionarily perfect enzyme.³² A component of the driving force for rapid binding of ACh is the high negative charge density of

TABLE I. Rate and Equilibrium Constants for Binding of Ligands and Substrates to AChE^a

compound	K_d , μM	k_{12} , $\text{M}^{-1} \text{s}^{-1}$
<i>N</i> -methylacridinium (1) ^b	0.149 (± 0.003)	$1.18 (\pm 0.03) \times 10^9$
<i>N</i> -methylacridinium ^c	<0.012	1.1×10^{10}
1-methyl-7-hydroxyquinolinium (2) ^b	0.37 (± 0.09)	$2.2 (\pm 0.2) \times 10^9$
acetylthiocholine (ATCh) ^c	<4.2	4.2×10^9

^a K_d is the enzyme-ligand dissociation constant; k_{12} is the ligand association rate constant. ^b Data are taken from ref 34. ^c Data are taken from ref 33. The association rate constants were calculated by least-squares extrapolation of the dependence of k_{12} on ionic strength to 0 ionic strength. K_d for *N*-methylacridinium is the measured value at the lowest ionic strength. K_d for ATCh is the K_m measured at the lowest ionic strength; k_{12} for ATCh is the least-squares-extrapolated k_E .

the AChE active site.³³ Rosenberry and Neumann used fluorescence temperature jump relaxation kinetics to measure the rate and equilibrium constants for association of *N*-methylacridinium (1) and *N*-methyl-7-



hydroxyquinolinium (2) with AChE at ~ 0.1 M ionic strength.³⁴ These values are contained in Table I, as are values extrapolated to zero ionic strength of k_{12} for *N*-methylacridinium binding and k_E for hydrolysis of ATCh. The rate constants in Table I are very high, and are consistent with diffusion-controlled interactions. The net charge of the AChE active site was determined from the ionic strength dependence of k_{12} for *N*-methylacridinium and k_E for ATCh; the respective values were $Z_E = -6.3$ and $Z_E = -9$. This large negative charge suggests that cationic ligands and ATCh (and also by analogy the physiological substrate ACh) bind to an enzyme surface area larger than the active site itself and proceed to the active site by diffusion on the surface of the enzyme. The very large value of k_E for ATCh at ionic strength = 0 ($k_E = 4.2 \times 10^9 \text{ M}^{-1} \text{ s}^{-1}$) is consistent with diffusion of substrate to the enzyme or along the enzyme's surface as the rate-determining step. This model is supported by the effects of viscosity on k_E for AChE-catalyzed hydrolysis of ATCh.³¹

TABLE II. Substrate Specificity of AChE

substrate	structure	rel k_E^a	ref ^b
acetylcholine	$\text{CH}_3\text{C}(\text{O})\text{OCH}_2\text{CH}_2\text{N}^+\text{Me}_3$	1.00	2, 38
acetylthiocholine	$\text{CH}_3\text{C}(\text{O})\text{SCH}_2\text{CH}_2\text{N}^+\text{Me}_3$	1.58	2, 37, 38
acetylselenocholine	$\text{CH}_3\text{C}(\text{O})\text{SeCH}_2\text{CH}_2\text{N}^+\text{Me}_3$	3.62	2, 38
acetylazacholine	$\text{CH}_3\text{C}(\text{O})\text{NHCH}_2\text{CH}_2\text{N}^+\text{Me}_3$	2.5×10^{-5}	39
(<i>N,N</i> -dimethylamino)ethyl acetate	$\text{CH}_3\text{C}(\text{O})\text{OCH}_2\text{CH}_2\text{N}^+\text{HMe}_2$	0.076	2, 41
(<i>N</i> -methylamino)ethyl acetate	$\text{CH}_3\text{C}(\text{O})\text{OCH}_2\text{CH}_2\text{N}^+\text{H}_2\text{Me}$	3×10^{-3}	2, 41
aminoethyl acetate	$\text{CH}_3\text{C}(\text{O})\text{OCH}_2\text{CH}_2\text{N}^+\text{H}_3$	1.6×10^{-4}	2, 41
3,3-dimethylbutyl acetate	$\text{CH}_3\text{C}(\text{O})\text{OCH}_2\text{CH}_2\text{CMe}_3$	0.025	44
propanoylcholine	$\text{CH}_3\text{CH}_2\text{C}(\text{O})\text{OCH}_2\text{CH}_2\text{N}^+\text{Me}_3$		2, 40
butanoylcholine	$\text{CH}_3\text{CH}_2\text{CH}_2\text{C}(\text{O})\text{OCH}_2\text{CH}_2\text{N}^+\text{Me}_3$		2, 40
phenyl acetate	$\text{CH}_3\text{C}(\text{O})\text{OC}_6\text{H}_5$	0.05	2, 19, 22, 27
<i>o</i> -nitrochloroacetanilide	$\text{ClCH}_2\text{C}(\text{O})\text{NHC}_6\text{H}_4\text{NO}_2\text{-}o$	2.6×10^{-3}	18, 20, 21, 35
indophenyl acetate	16 ^c	1.3×10^{-3}	2, 25, 45, 93
tropolone acetate	17 ^c	0.76	35
ethyl acetate	$\text{CH}_3\text{C}(\text{O})\text{OCH}_2\text{CH}_3$	7.9×10^{-6}	2, 27
<i>p</i> -methoxyphenyl formate	$\text{HC}(\text{O})\text{OC}_6\text{H}_4\text{OMe-}p$	0.08 ^d	20

^a The value of k_E for ACh is $1.6 \times 10^8 \text{ M}^{-1} \text{ s}^{-1}$; see Table IX of ref 2 and references cited therein. This table is not meant to be an exhaustive exposition of the range of AChE substrates. ^b The references in bold print are those from which relative k_E values were calculated. ^c Numbers refer to structures displayed elsewhere in this review. ^d Calculated from k_E values of *p*-methoxyphenyl formate and phenyl acetate in ref 19 and 20.

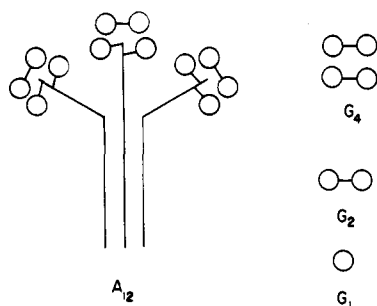
Schowen¹⁰ calculated catalytic accelerations wrought by AChE by comparing ΔG^\ddagger calculated from k_E of AChE-catalyzed hydrolysis of ACh with ΔG^\ddagger values for neutral, basic, and acidic hydrolyses of ACh. The enzyme reaction is accelerated vs. these three reactions by about 10, 8, and 13 orders of magnitude, respectively. These catalytic accelerations correspond to transition-state binding energies of -13.9 , -10.6 , and $-17.3 \text{ kcal mol}^{-1}$, respectively. These calculations attest to the catalytic power of AChE.

AChE is a promiscuous catalyst, as the broad substrate specificity outlined in Table II shows. The enzyme catalyzes reactions of aryl esters,^{2,19,20,22,27} anilides,^{18,20,21,35,36} thioesters,^{2,37,38} amides,³⁹ selenoesters,³⁸ and acyl homologues^{2,40} and *N*-demethylated⁴¹ analogues of ACh. Specificity (i.e., k_E) is highest for ACh, ATCh, and acetylselenocholine. AChE is an order of magnitude less specific for phenyl acetate.^{2,27} The amide analogue of ACh, acetylazacholine, provides an interesting case in point. This substrate has $k_E = 4 \times 10^3 \text{ M}^{-1} \text{ s}^{-1}$,³⁹ about five orders of magnitude smaller than k_E for ACh. Since the hydrolytic reactivity of amides is about 10^4 - to 10^5 -fold less than that of structurally similar esters,⁴² the catalytic acceleration that AChE brings to bear in hydrolyzing acetylazacholine is similar to that for the physiological substrate ACh. Therefore, even though k_E for acetylazacholine is much smaller than for ACh, the enzyme's catalytic power toward these two substrates is nearly the same. This comparison underscores that use of alternate substrates can be informative in investigations of AChE catalysis. As shall be seen later, investigations of aryl ester and anilide hydrolyses have begun to reveal the dynamic and chemical anatomy of AChE catalysis.

II. AChE Structure

A. Tertiary and Quaternary Structure

AChE is a polymorphic enzyme *in vivo*.^{2,46,47} The enzyme consists of globular catalytic subunits that have masses of 70–80 K. The assembly of these catalytic subunits in oligomeric structures has been reviewed recently by Rosenberry⁴⁶ and by Massoulié and Bon.⁴⁷ Salient features of the supramolecular organization of AChE subunits will be summarized herein before

CHART II. Representation of Asymmetric and Globular Forms of AChE

turning to the more germane (for this review) primary structure and active site structure and dynamics of the enzyme.

Except for the erythrocyte enzyme, catalytic AChE subunits appear in two major classes of oligomers: globular forms and asymmetric forms (denoted by G and A, respectively). The various constituents of the globular and asymmetric classes are outlined in Chart II. Globular forms include G_1 , G_2 (a disulfide-linked dimer of identical catalytic subunits), and G_4 (a tetramer). Each G subunit contains a single active site. Asymmetric forms contain three major structural domains: catalytic subunits, collagen-like tail, and non-collagenous tail. The collagen-like tail is rich in glycine, hydroxyproline, and hydroxylysine, is degraded by collagenase, and, hence, likely consists of a triple helix of polypeptide units.⁴⁸ Each polypeptide unit terminates with a short noncollagenous polypeptide (~8K molecular mass^{46,48}) that makes two disulfide bonds to individual globular subunits. An extra catalytic dimer, in which subunits are disulfide linked, associates with the disulfide-bonded pair of catalytic subunits at the end of the noncatalytic tail polypeptide. Among the asymmetric forms of AChE are those designated A_{12} , A_8 , and A_4 that have twelve, eight, and four catalytic subunits, respectively. The molecular organization of the A_{12} oligomer is depicted in Chart II. The A_8 and A_4 forms have noncatalytic polypeptide chains that are devoid of one and two catalytic tetramers, respectively. Polymorphic AChEs, including asymmetric forms, are found in fish electric organs, avian muscle, mammalian skeletal muscle, and in rat vagus nerve, smooth muscle, and heart muscle.⁴⁶ Though AChE is polymorphic, activities of catalytic subunits in the asymmetric and globular forms of the enzyme are similar.⁴⁹

In contrast to the sources just discussed, some cells produce predominantly or exclusively globular AChEs, as discussed in the recent review by Rosenberry.⁴⁶ Of these, the structure of the human erythrocyte enzyme has been studied in some detail. This enzyme is viewed as a membrane-bound, disulfide-linked dimer^{46,50} of identical 75K subunits (i.e., a G_2 form). Brimijoin and Mintz⁵¹ used monoclonal antibodies to investigate the epitope distribution and cellular location of human erythrocyte AChE. Five of six antibodies interact with intact washed erythrocytes, which suggests that most of the enzyme dimer is external to the cell membrane. The failure of the sixth antibody to react could signal that an AChE epitope is localized in or near the external lipid layer of the cell membrane. The structure, cellular location, and catalytic mechanism of erythrocyte AChE are of general interest, since monoclonal antibodies have

been used to demonstrate homologies among erythrocyte, neuromuscular junction, and brain enzymes.^{52,53}

Rosenberry and co-workers⁵⁴ called human erythrocyte AChE an "amphipathic" protein, which consists of a large hydrophilic catalytically active domain and a small hydrophobic domain that is responsible for membrane binding. The purified enzyme is a disulfide-linked dimer in nonionic detergent solutions but forms soluble aggregates when detergent is absent. Enzyme monomers produced by disulfide reduction maintain their detergent-binding properties and tendency toward aggregation. Treatment of purified human erythrocyte AChE (either as enzyme aggregates or as complexes with phospholipid liposomes or detergent micelles) with papain releases a short hydrophobic peptide of 3.1K mass. The remaining hydrophilic domain is scarcely smaller than the intact 75K catalytic subunit, no longer binds to TX100 micelles or phospholipid liposomes, does not self-aggregate, but retains full catalytic activity.^{54,55} Hence, the papain-released hydrophobic domain is the membrane-binding segment of the enzyme and must constitute the amino or carboxyl terminal region. The hydrophobic domain was identified as the carboxyl terminal fragment by radiomethylation of amino groups of the intact protein with [¹⁴C]H₂CO and NaCNBH₃.^{54,56} This procedure labeled the amino terminus, which was identified as glutamate or arginine (detected in a 2 to 1 ratio, with a summed stoichiometry of 1 amino acid/AChE subunit⁵⁶). The hydrophobic carboxyl terminal fragment contains 1 mol each of histidine, glycine, glucosamine, palmitate, 22:4 + 22:5 fatty acids,⁵⁷ and 2 mol of ethanolamine. The fragment is therefore a proteolipid, whose sequence is His-Gly-ethanolamine-Z.⁵⁶⁻⁵⁸

The human erythrocyte enzyme is not unique among AChEs in having a glycolipid-containing hydrophobic membrane-binding domain. The membrane-binding domain of the dimeric enzyme from *Torpedo californica* is cleaved by phosphatidylinositol-specific phospholipase C (PIPLC),⁵⁹ and the sheep platelet membrane-bound AChE is similarly cleaved by PIPLC.⁶⁰

B. Primary Structure

The amino acid sequence of *T. californica* AChE, which was determined from the requisite cDNA sequence, was recently reported by Schumacher et al.⁶¹ They describe several features of the sequence that are noteworthy: (1) The cDNA sequence indicates that there is a continuous stretch of 13 amino acids that likely comprise a leader sequence and that is missing in the native enzyme. This peptide is rich in hydrophobic amino acids, which is consistent with a putative membrane-spanning function. Therefore, catalytic subunits of *T. californica* AChE are likely synthesized as proproteins that are cleaved to the native subunits before or during export of the enzyme from the cell. (2) The native enzyme contains a single polypeptide of 575 amino acids and has a calculated M_r of 65 612. Since catalytic subunits of the native enzyme contain 7–8% carbohydrate, the sequence produces a M_r that is consistent with M_r 70–80K determined by electrophoresis of purified catalytic subunits of various AChEs.^{46,47} (3) Ser²⁰⁰ in the sequence is labeled with [³H]diisopropyl-fluorophosphate, and hence comprises the nucleophilic element of the active site. The peptide sequence about

CHART III. Comparison of Active Site Sequences of AChE and Other Serine Enzymes^a

protein	amino acid sequence
Torpedo californica AChE ⁶⁶	H ₂ N-Thr-Val-Thr-Ile-Phe-Gly-Glu-Ser-Ala-Gly-Gly-Ala-Ser-Val-Gly-Met-His-Ile-Leu-Ser-COOH
Electrophorus electricus AChE ⁶⁷	-Gly-Gly-Glu-Ser-Ser-Glu-Gly-Ala-Ala-Gly-
equine aliesterase ⁶⁶	-Phe-Gly-Glu-Ser-Ala-Gly-Ala-Ala-Ser-
human serum BuChE ^{b,66}	-Ser-Val-Thr-Leu-Phe-Gly-Glu-Ser-Ala-Gly-Ala-Ala-Ser-Val-Ser-Leu-His-Leu-Leu-Ser-
bovine trypsinogen ⁶⁶	-Lys-Asp-Ser-Cys-Gln-Gly-Asp-Ser-Gly-Gly-Pro-Val-Val-Cys-Ser-Gly-Lys-
porcine trypsin ⁶⁶	-Lys-Asp-Ser-Cys-Gln-Gly-Asp-Ser-Gly-Gly-Pro-Val-Val-Cys-Asn-Gly-Gln-
bovine milk LpL ^{c,68}	-Ile-Gly-Ile-His-Trp-Gly-Gly-Ser-Pro-Asn-Gln-Lys-Asn-Gly-Ala-Val-Phe-Ile-Asn-

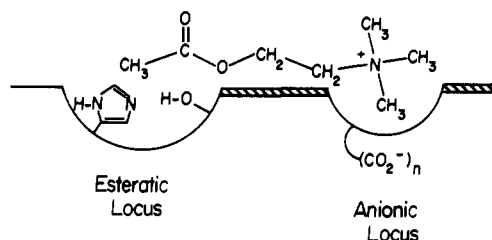
^a The arrow denotes the position of Ser²⁰⁰ in the sequence of *T. californica* AChE.⁶⁶ ^b BuChE = Butyrylcholinesterase. ^c LpL = Lipo-protein lipase.

the active site serine is shown in Chart III and is compared to active site sequences of serine proteases and other esterolytic enzymes. (4) The serine proteases contain a catalytic triad of precisely oriented active site amino acids (His⁵⁷, Asp¹⁰², and Ser¹⁹⁵ in chymotrypsin;⁶² Asp³², His⁶⁴, and Ser²²¹ in subtilisin⁶³). This triad has been called the charge relay system⁶⁴ and stabilizes chemical catalytic transition states via coupled proton transfers. The active site serine of AChE is in a position in the sequence that is close to that of the serine proteases. However, the AChE sequence does not contain putative active site His or Asp residues that are positioned similarly to those of the serine proteases. Therefore, the oft-used serine protease analogy is not supported by comparisons of primary structures.

The pattern of disulfide bonds and the consequent protein folding they produce in *T. californica* AChE are also different from those of mammalian and bacterial serine proteases.⁶⁵ AChE contains three pairs of disulfide bonds and, hence, three disulfide loops: Cys⁶⁷-Cys⁹⁴, Cys²⁵⁴-Cys²⁶⁵, and Cys⁴⁰²-Cys⁵²¹. The comparison of amino acid sequences in Chart III also underscores the structural distinctness of AChE and serine proteases.⁶⁶ There is only limited homology between the two classes of enzymes in the active site regions. However, no significant homology extends through the rest of the sequences. The closest sequence homology with other serine enzymes is with carboxylesterases and aliesterases; Chart III shows considerable homology in the active site regions of Torpedo AChE and equine aliesterase. Torpedo AChE also shows considerable active site region homology with human serum BuChE, which suggests that the reaction dynamics of these two enzymes may be similar. AChE and BuChE also display homology in their amino terminal sequences,⁶⁶ though not of the degree displayed by the active center regions in Chart III. The chart also shows that the active center region of bovine milk LpL⁶⁸ has almost nil homology with those of AChE and other serine enzymes. Hence, it seems that nucleophilic catalysis by serine is such a successful element of esterolytic enzyme catalytic power that it has been widely selected by convergent evolution. However, the comparisons among AChE, serine proteases, and LpL in Chart III suggest that the catalytic mechanisms of these enzymes, though similar, probably have important differences.

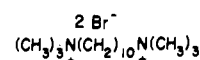
C. Active Site Structure

The AChE active site consists of three major domains: (1) an esteratic locus, comprised of the active site serine,^{66,67} (2) an anionic locus that is ≥ 4.7 Å from

CHART IV. Representation of the Active Site of AChE^a

^a $n = 6-9$. Cross-hatched areas denote sites of hydrophobic interaction.

the esteratic serine, where the quaternary ammonium pole of ACh and of various active site ligands binds;^{2,3,25} (3) a hydrophobic region that is contiguous with or near the esteratic and anionic loci and that is important in binding aryl substrates and active site ligands. A stylized diagram of the domains of the active site is given in Chart IV. A fourth domain in the enzyme binds cationic ligands, such as gallamine, *d*-tubocurarine, and decamethonium (3). This domain is >20



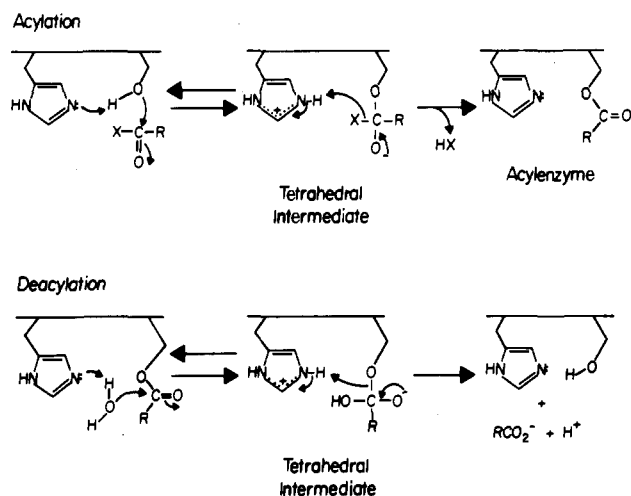
3

Å from the active site⁶⁹ and has been called the peripheral anionic site.^{70,71} Ligand occupation of the peripheral anionic site frequently changes the conformation of the active center.^{72,73} The four domains of AChE conspire to produce the complex reaction dynamics and active site conformational dynamics that are hallmarks of the enzyme. Below, some salient features of interactions in each of these domains are discussed.

1. Esteratic Locus

In addition to Ser²⁰⁰, the esteratic locus of AChE is thought to contain the imidazole functionality of histidine,^{2,3,25,74,75} which likely functions as a general acid-base catalyst in the formation and decomposition of tetrahedral intermediates, as outlined in Scheme III. The active site histidine is thought to have an intrinsic $\text{p}K_a \sim 6.3$.^{2,25,76,77} The rate of formation of tetrahedral intermediates will depend on the basic form of the histidine and, hence, pH-rate profiles for AChE reactions should give $\text{p}K_a$ values of about 6.3. This is the case for k_E and k_{ES} of AChE-catalyzed hydrolysis of ACh^{2,27,76} and for k_{ES} of ATCh⁷⁷ and phenyl acetate^{27,76,77} hydrolyses. However, various uncharged substrates have pH- k_E profiles that give $\text{p}K_a$ values that are well below 6.3.^{2,18-21,27,76,77} In addition, reactivity of neutral carbamylating reagents with the AChE active site de-

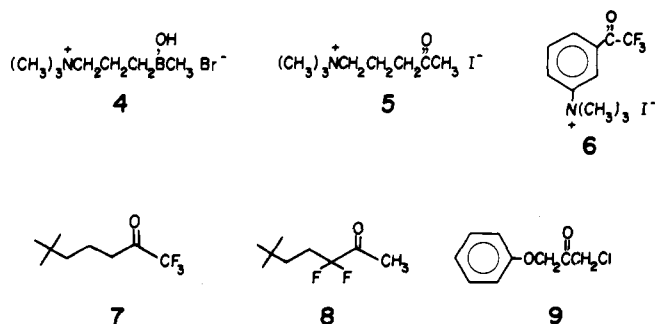
SCHEME III. Chemical Mechanism for AChE Catalysis



depends on a pK_a well below 6.3.⁷⁸ A quantitative rationale for this pH-rate behavior will be developed in the reaction dynamics section of this review.

The mechanism of Scheme III bears some resemblance to the serine protease mechanism,⁷⁻⁹ save that no mention is made of an aspartate or glutamate residue that would complete an AChE "charge relay" system. Such a system has been shown to operate for a wide range of serine protease reactions when transition-state proton bridges are directly studied by measurements of solvent isotope effects and proton inventories.^{17,79-82} The use of these probes to determine that AChE operates as a simple general acid-base catalyst (i.e., transition states involve single-proton bridges, as outlined in Scheme III) will be detailed later in this review.

Various observations support the mechanism of Scheme III. An acetylzyme intermediate accumulates during AChE-catalyzed turnover of ACh and ATCh.²⁶ The acetylzyme is rapidly hydrolyzed, with a $t_{1/2} < 0.1$ ms.^{2,26} The enzyme is readily inhibited by carbamates and by acyl halides of substituted phosphoric, phosphonic, carbamic, and sulfonic acids.^{2,3,25} These inhibitions produce carbamyl-, phosphoryl-, phosphonyl-, and sulfonylzyme analogues of the acylzyme intermediate, which turn over very slowly if at all. Though there is no direct evidence for tetrahedral intermediates in the AChE mechanism, the enzyme shows esteratic locus complementarity for inhibitors that probably bind in modes that structurally mimic tetrahedral intermediates. For example, *N,N,N*-trimethylammonium boronic acid (4) is a potent



reversible inhibitor of *Electrophorus Electricus* AChE-catalyzed hydrolysis of ACh, with a $K_i \sim 20$ nM at pH 7.5.⁸³ In contrast, the ketone analogue 5 binds

2500-fold less tightly to the enzyme.⁸⁴ Compound 4 probably binds at the esteratic locus with the γ -OH of serine bonded to the electrophilic boron, thereby generating a tetrahedral adduct that structurally mimics the tetrahedral intermediate in the acylation stage of catalysis (cf. Scheme III). This mode of binding accounts for the potent inhibition of serine proteases by boronic acids.⁸⁵⁻⁸⁸ *m*-(*N,N,N*-Trimethylammonio)trifluoroacetophenone (6) is a slow, tight-binding inhibitor of AChE;⁸⁹ the concentration of 6 that inactivates the enzyme by 50% after a 30-min incubation is 13 nM. Fluoro ketone analogues 7 and 8 of ACh, with a *tert*-butyl replacing the trimethylammonio function, have been synthesized by Gelb et al.⁹⁰ These compounds are competitive inhibitors, with respective K_i values of 16 and 1.6 nM. Inhibitor 8 is the most potent reversible AChE inhibitor known. 1-Chloro-3-phenoxy-2-propanone (9) is a rapid, reversible AChE inhibitor, with $K_i = 0.85$ μ M.⁹¹ Halo ketones 6-9 owe their potency as AChE inhibitors to probable formation of tetrahedral hemiketal adducts with the active site serine.

The Scheme III mechanism is by no means the only one that can be written that involves the active site histidine in general acid-base catalysis. For example, the histidine may catalyze a "proton switch"⁹² by transferring the proton from the active site serine or from H₂O to the oxyanion of the incipient tetrahedral intermediates of the acylation and deacylation stages of catalysis, respectively. Furthermore, compelling evidence that histidine is the active site function that has a $pK_a = 6.3$ and that is involved in general acid-base catalysis is lacking. Covalent labeling and consequent active site peptide isolation and structure elucidation would provide the requisite support for histidine's putative role in AChE catalysis. In addition, X-ray structural characterization of native AChE and of modified AChEs, such as carbamylenzymes or complexes with transition-state analogues, should one day provide a firmer basis for the postulation of detailed mechanistic models. Though such structural information is lacking, the Scheme III mechanism serves as a useful framework for interpretation of the results of various mechanistic probes, as shall be seen later.

2. Anionic Locus

The anionic locus of the AChE active site is ≥ 4.7 Å from the serine hydroxyl of the esteratic locus,²⁵ and contains multiple negative charges,³³ as indicated in Chart IV. An anionic locus in the active site is signalled by the interaction of various types of compounds with AChE, including:^{2,3,25} (1) aromatic cations, (2) tetraalkylammonium salts, (3) aziridinium covalent modifying reagents,^{93,94} (4) bisquaternary ammonium compounds that span the peripheral anionic locus and the anionic locus of the active site, (5) pyridinium reactivators of active site phosphorylated and phosphonylated AChEs.

Controversy has arisen over the last 7 years concerning whether there is a true anionic locus in the active site. Hasan et al.⁴⁴ proposed that the locus on the enzyme that binds the quaternary functionality of ACh and various inhibitors is a hydrophobic trimethyl binding site. They based this model on the fact that for a series of substrates $XCH_2CH_2OCOCH_3$ ($X =$

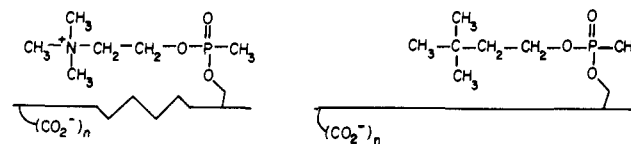
TABLE III. Comparison of Charged and Uncharged Reversible Inhibitors of AChE^a

entry	structure	K_i , mM
A	$\text{Me}_3\text{N}^+\text{CH}_2\text{CH}_2\text{CH}_2\text{COCH}_3 \text{ I}^-$	0.022
B	$\text{Me}_3\text{CN}^+\text{H}_2\text{CH}_2\text{CH}_2\text{COCH}_3 \text{ Cl}^-$	0.16
C	$\text{Me}_3\text{CSCH}_2\text{CH}_2\text{COCH}_3$	0.40
D	$\text{Me}_2\text{N}^+\text{HCH}_2\text{CH}_2\text{CH}_2\text{COCH}_3 \text{ Cl}^-$	0.77
E	$\text{Me}_3\text{COCH}_2\text{CH}_2\text{COCH}_3$	1.6
F	$\text{Me}_2\text{CHN}^+\text{H}_2\text{CH}_2\text{CH}_2\text{COCH}_3 \text{ Cl}^-$	2.0
G	$\text{Me}_2\text{CHOCH}_2\text{CH}_2\text{COCH}_3$	4.8
H	$\text{Me}_2\text{CHCH}_2\text{CH}_2\text{CH}_2\text{COCH}_3$	2.8
I	$\text{Me}_3\text{N}^+\text{CH}_2\text{CH}_2\text{CH}_2\text{B}(\text{OH})\text{CH}_3 \text{ Br}^-$	2×10^{-5}

^a All K_i values are for competitive inhibition of AChE-catalyzed hydrolysis of ACh. Entries A–G are from ref 96. Entry H is from ref 97. Entry I is from ref 83.

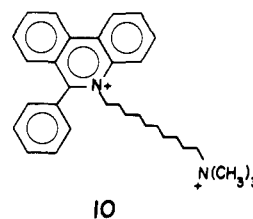
nonpolar, polar, and cationic groups) AChE reactivity increased with increasing OH⁻-catalyzed hydrolytic reactivity of the esters. In addition, they showed a correlation of the partial molal volume of the β -substituent X and the second-order rate constant k_E for AChE catalysis. The correlation with hydrolytic reactivity is not surprising, since both reactions involve attack of oxygen nucleophiles on the carbonyl carbon of substrates. The correlation of β -substituent volume with AChE reactivity is not particularly revealing, since the transfer of hydrocarbons in a homologous series from aqueous solution to lipidlike organic phases correlates with hydrocarbon surface area.⁹⁵ Since increasing volume of the β -substituents of AChE substrates is directly proportional to increasing β -substituent surface area, the correlation reported by Hasan et al. may indicate nothing more than that for charged and uncharged substrates the second-order rate constant k_E gauges (among other enzyme–substrate interactions) transfer of substrate from solution to a lipidlike environment at the AChE active site. There is no reason to assert, a priori, that a *tert*-butyl substituent binds in the same lipidic active site environment as does a trimethylammonio substituent.

Hasan et al.⁹⁶ also compared the effects of various inhibitors on AChE-catalyzed hydrolysis of ACh and of the uncharged isosteric analogue 3,3-dimethylbutyl acetate (DMBA). Table III gives the structures and competitive inhibition constants of some of the inhibitors described by Hasan et al.⁹⁶ (entries A–G). Comparison of inhibitors A and D and inhibitors B and F shows that removal of a methyl group from the quaternary ammonio and *tert*-butyl functions reduces inhibitor potency 10- to 35-fold, which supports the importance of trimethyl substitution distal to the carbonyl. Movement of the + charge closer to the carbonyl (compare A and B) results in \sim 7-fold reduction in inhibitor potency. Hasan et al. compare K_i values for B, C, and E and consequently assert that the + charge only contributes 3- to 10-fold to binding. However, one could argue that C and E are uncharged analogues of A, and hence, the + charge contributes 18- to 73-fold to binding. There are two additional shortcomings in the comparisons that Hasan et al. make: (1) Uncharged and charged inhibitors may not bind equivalently to the active site. For example, 6-methyl-2-heptanone (entry H) binds with roughly the same affinity as E and G and only 7-fold less well than C. However, Dafforn et al.⁹⁷ have shown that aliphatic ketones are 30- to 170-fold less effective in protecting AChE against inactivation by the active site serine modifying reagent methyl-

CHART V. Charged and Neutral Methylphosphono-AChE Complexes

sulfonyl fluoride than expected from their K_i values for inhibition of ACh hydrolysis. Hence, it is doubtful that all the uncharged inhibitors in Table III interact appreciably with the esteratic locus of the active site. (2) Relative binding of inhibitors A–G may be a poor reflection of the importance of substrate + charge on binding in the transition state. This point is underscored by the fact that I binds \sim 1000-fold more tightly than does A. If A is a transition-state analogue,⁹⁸ it is not a very good one. Uncharged analogues of I would provide a much better comparison for the effect of + charge on AChE catalysis. Perhaps the most germane comparison is that of k_E values. As Fersht⁹⁹ has shown, k_E reflects the strength of interaction of enzyme and substrate in the transition state. As discussed earlier in this review, k_E is the rate constant for conversion of free E + S to the rate-determining acylation transition state. For ACh and DMBA Hasan et al.⁴⁴ measured k_E values of 4.8×10^7 and $1.2 \times 10^6 \text{ M}^{-1} \text{ s}^{-1}$, respectively. Therefore, + charge has a 40-fold effect on substrate binding where it counts most, in the transition state.

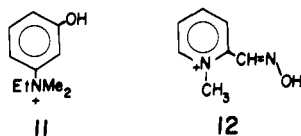
Clearly, a method is required to resolve the controversy over whether there is an anionic locus or a trimethyl-binding locus in the AChE active site. Recent experiments by Berman and Decker¹⁰⁰ appear to resolve the issue. They inhibited *T. californica* AChE with closely isosteric β -(trimethylamino)ethyl and 3,3-dimethylbutyl methylphosphonofluoridates. These compounds phosphonylate the active site Ser²⁰⁰ to produce tetrahedral adducts that structurally mimic the tetrahedral intermediate in the acylation stage of catalysis (compare Scheme III and Chart V). Since enzymes catalyze reactions by binding more tightly to transition states than to other ES complexes,^{10,101} it is reasonable to expect that AChE binds tightly to high-energy tetrahedral intermediates and, by analogy, to tetrahedral phosphonyl complexes. Therefore, phosphonyl-AChEs should adopt catalytically relevant conformations. If the anionic locus is actually an uncharged trimethyl binding site,^{44,96,102} the quaternary ammonio and trimethyl functions of the respective phosphonyl enzymes should occupy the same site. Binding of various ligands to the phosphonyl enzymes and to native AChE shows that this is not so. The fluorescent diquaternary ligand decidium (10) binds to the native enzyme with its aro-



matic moiety binding to the peripheral anionic site and the trimethylamino function in the active site.¹⁰³ The dissociation constant of the dimethylbutyl methylphosphono-AChE complex with decidium ($K_d = 54 \pm$

12 nM) is nearly the same as that for the complex with the native enzyme ($K_d = 21 \pm 2$ nM), whereas that for the charged methylphosphono-AChE complex is 100-fold higher ($K_d = 4.3 \pm 1$ μ M). These results are consistent with occupation of an active site anionic locus in the charged methylphosphono-AChE complex but not in the uncharged complex, as shown schematically in Chart V. That the anionic locus of the active site is not occupied in the uncharged complex is supported by the fact that various *n*-alkyl mono- and bisquaternary ligands bind with the same affinity to native AChE and to dimethylbutyl methylphosphono-AChE.¹⁰⁰ This is not the case, however, for pyrenebutyl methylphosphono-AChE, to which decidium binds with 100-fold lower affinity relative to binding to native AChE.¹⁰⁰ In this case, the pyrenebutyl moiety extends far enough to overlap the anionic locus of the active site. Therefore, though the inhibitor portions of the charged and uncharged methylphosphono-AChEs are sterically equivalent, the conformations of AChE that accommodate the respective functionalities are not.

There is no doubt that Ser²⁰⁰ is covalently labeled in the uncharged complex, since binding thereto of cations such as edrophonium (tensilon, 11) and *N*-methyl-



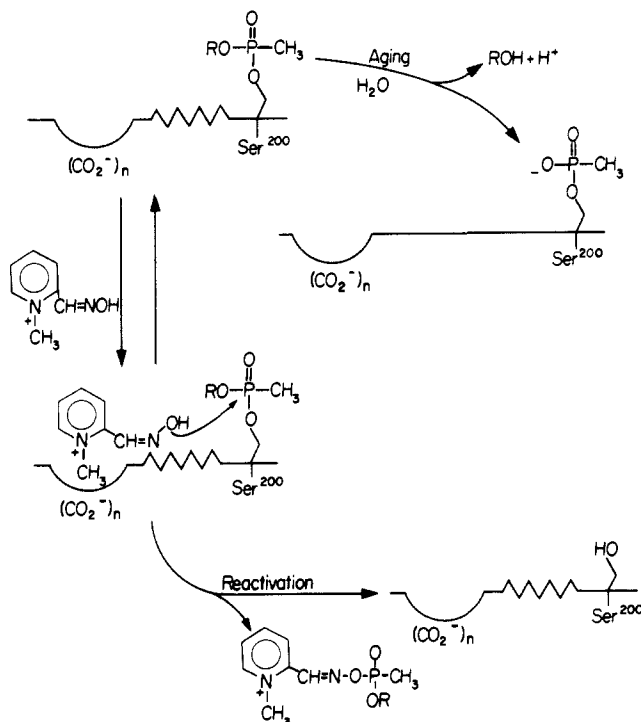
acridinium (1), which are known to bind at the anionic locus of the active site,^{2,3,104} is greatly reduced vs. binding to the native AChE.¹⁰⁰ The different effects of the uncharged methylphosphono function on binding of active-site-directed cations vs. alkyl mono- and bisquaternary ligands and decidium is consistent with either of the following explanations: (1) heterogeneity of cation binding sites near the active site serine,¹⁰⁰ (2) different modes of anionic locus binding of the trimethylammonio functions of decidium and alkyl mono- and bisquaternary ligands vs. the cationic aromatic ligands. The first explanation is supported by the estimate of Nolte et al.³³ of ≥ 6 negative charges in the anionic locus of the AChE active site. The latter explanation is consistent with the effects of aromatic cations such as *N*-methylacridinium (1) and 1-methyl-2-(hydroxyiminomethyl)pyridinium (2-PAM, 12) on AChE-catalyzed hydrolysis of alkyl acetates.¹⁰⁵ *N*-methylacridinium accelerates AChE-catalyzed hydrolysis of methyl acetate (3-fold), ethyl acetate (5-fold), and *n*-propyl acetate (2-fold) but inhibits hydrolysis of *n*-butyl acetate. 2-PAM shows the same trend, though the effects are not as great. Hence, when the substrate is large enough (i.e., *n*-butyl acetate), the binding domains of ligands and substrate overlap and inhibition occurs. A similar overlap of binding domains probably accounts for the greatly reduced binding of tensilon and *N*-methylacridinium to dimethylbutyl methylphosphono-AChE vs. binding to native AChE.¹⁰⁰ Binding of decidium and alkyl mono- and bisquaternary ligands to the anionic locus of the active site may not involve overlap of binding domains with the uncharged methylphosphono function. At the present time, there are no experimental data that clearly distinguish between the two explanations offered herein for the various effects on ligand binding of dimethylbutyl me-

thylphosphonylation of AChE.

The experiments of Berman and Decker¹⁰⁰ that are discussed in the preceding two paragraphs provide a potential structural rationale for the induced fit that Rosenberry^{2,27} suggested is rate controlling in the acylation stage of AChE-catalyzed hydrolyses of neutral esters. The conformation of the β -(trimethylammonio)ethyl methylphosphono-AChE complex mimics the tetrahedral intermediate in the acylation stage of AChE-catalyzed hydrolysis of cationic substrates and involves simultaneous interaction at the anionic and esteratic loci of the active site (cf. Scheme III and Chart V). This conformation must be rapidly induced during AChE-catalyzed hydrolysis of ACh, perhaps by the developing interaction of the anionic locus with the trimethylammonio pole of ACh, since the acylation stage of this reaction is rate limited by diffusion.^{2,31,33} Consequently, it is reasonable to assert that the AChE conformation that is induced on ACh binding is optimally potent catalytically and, thus, must align active site functionalities for maximal stabilization of the chemical transition states that follow. The conformation of the enzyme in the dimethylbutyl methylphosphono-AChE complex, on the other hand, mimics the tetrahedral intermediate in the acylation stage of neutral substrate turnover and leaves the anionic locus of the active site open, as discussed by Berman and Decker¹⁰⁰ and shown schematically in Chart V. Since the quaternary ammonium pole is not available to drive the conformation change during acylation with neutral substrates, this step may become partly or solely rate determining.

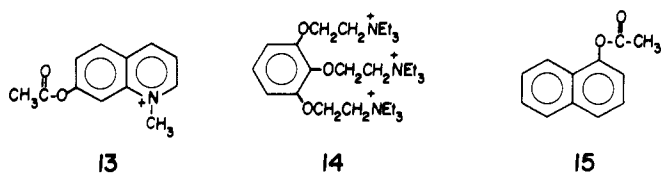
This model for active site dynamics during the acylation stage of catalysis is consistent with the demonstrated conformational flexibility of the active site. Berman and Decker¹⁰³ used the fluorescent ligand decidium (10) to characterize the effect of aging of cycloheptyl methylphosphono-AChE (cf. Scheme IV) on the conformation of the active center. Aged AChE is insensitive to reactivation by nucleophiles such as 2-PAM that bind at the anionic locus of the active site.^{2,3} Native and aged enzymes bind decidium with nearly equal affinity ($K_d \sim 20$ nM). Binding of active site and peripheral site ligands and ligands that span both sites was determined from fluorescence changes that accompany displacement of decidium by the ligands. Binding of *N*-methylacridinium (1) and phenyltrimethylammonium (anionic locus of the active site) and of propidium (peripheral site) is not very different for aged and native AChEs. However, binding of edrophonium (11) to the anionic locus of the active site is decreased 130-fold in the aged vs. the native enzyme, which is consistent with a conformational change that disrupts an H bond between the inhibitor and an acceptor residue in the active site.¹⁰⁶ Berman and Decker¹⁰³ proposed that in the aged enzyme the distance between the negatively charged methylphosphonyl-Ser²⁰⁰ and the anionic locus of the active site has increased because of charge-charge repulsion. The 76-fold enhancement of binding of decamethonium (3, spans peripheral anionic and active sites) at low ionic strength to the aged vs. the native enzyme also demonstrates that aging changes the protein's conformation.

Amitai et al.¹⁰⁷ suggested that nonaged and aged pyrenebutyl phosphoryl-AChEs are conformationally

SCHEME IV. Aging and Reactivation of Methylphosphono-AChE (R = Cycloheptyl)


different. An increased distance between Ser²⁰⁰ and the anionic locus also explains the insensitivity of aged AChE to reactivators such as 2-PAM (12). Berman et al.¹⁰⁸ used steady-state and time-correlated fluorescence to characterize the rotational mobilities of various AChE ligands. Steady-state polarizations of the pyrenebutyl methylphosphono-AChE complex with tetrameric AChE yielded a rotational correlation time of ~400 ns. Anisotropy decay of the propidium-AChE complex, wherein the peripheral anionic site is occupied, yielded a rotational correlation time of ~150 ns. Similar experiments for active-site-modified (dansylsulfonamido)pentyl and pyrenebutyl methylphosphono-AChEs gave rotational correlation times of ~300 ns. Anisotropy decay for the latter probe was biphasic, however, and yielded a second rotational correlation time of 18 ns. These correlation times indicate that the various probes reorient not only via rotation of the protein subunits but also via internal motion of the active site or peripheral site.

Rosenberry and Bernhard¹⁰⁹ characterized competitive and uncompetitive inhibitions of AChE-catalyzed hydrolyses of ACh, *N*-methyl-7-acetoxyquinolinium iodide (13) and 1-naphthyl acetate. Competitive in-

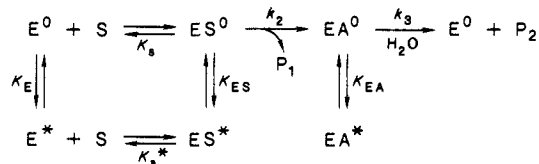


hibition dissociation constants were similar for the reactions of the three substrates in the presence of various inhibitors, including: flaxedil (14), *N*-methyl-5- and 7-hydroxyquinolinium iodides (2), 2-PAM (12), decamethonium bromide (3), *N*-methyl-5- and 7-acetoxyquinolinium iodides (13), 1-naphthyl acetate (15), 1-

TABLE IV. Synergistic Inhibition by Naphthyl Ligands of AChE-Catalyzed Hydrolysis of *N*-Methyl-7-acetoxyquinolinium Iodide (13)^a

inhibitor	K_u , mM	K_c , mM	K_c/K_u
1-naphthyl acetate	0.039 (± 0.002)	0.8 (± 0.1)	20 (± 3)
1-naphthol	0.31 (± 0.02)	1.7 (± 0.5)	5.5 (± 1.7)
1-naphthylamine	0.54 (± 0.06)	1.3 (± 0.3)	2.4 (± 0.7)

^aData are taken from ref 109.

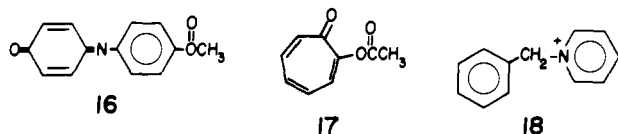
SCHEME V. Conformational Equilibrium Model for AChE Catalysis and Interaction with Inhibitory Ligands


naphthol, and ACh. Furthermore, pairs of substrates competitively inhibit each other with inhibition constants that equal their respective K_m values, which establishes that the three substrates, though structurally diverse, are hydrolyzed at a common active site. Flaxedil binds to the peripheral anionic site.¹⁰⁶ Hence, both competitive and uncompetitive inhibitions by flaxedil must be mediated by relay of conformational change from the peripheral site to the active site. An important finding of this study is the synergistic binding effect of pairs of inhibitors. Examples are given in Table IV and show that inhibitor binding in ternary complexes with the cationic substrate 13, itself an inhibitor of ACh and 1-naphthyl acetate hydrolyses, is tighter than in binary complexes, as reflected in K_c/K_u . Rosenberry and Bernhard¹⁰⁹ interpret this binding synergy and other observations in terms of conformational plasticity of the AChE active site, as represented by the mechanism of Scheme V. ACh, flaxedil, and the hydroxyquinolinium iodides interact with E⁰, ES⁰, and EA⁰, while 2-PAM and the acetoxyquinolinium iodides interact with E^{*}, ES^{*}, and EA^{*}, which are catalytically inactive. The inactive conformation is envisioned as separating the esteratic and anionic loci of the active site, which enables simultaneous interaction of the respective sites with naphthalene derivatives and aromatic cations. This model facilitates rationalization of synergistic competitive inhibition of ACh turnover by 2-PAM and 1-naphthyl acetate,¹⁰⁹ uncompetitive inhibition of acylenzyme turnover,^{2,110,111} and acceleration of alkyl acetate turnover by aromatic cations that bind at the anionic locus of the active site.^{105,112} However, Rosenberry and Bernhard¹⁰⁹ point out that the mechanism of Scheme V is not solely capable of explaining these kinetic behaviors. A model in which ligands induce the E⁰ and E^{*} conformations is equally viable.

The gist of the discussion in this section of the review is not only that AChE has a multifunctional active site comprised of esteratic and anionic loci, but also that AChE possesses conformational flexibility of catalytic significance. This conformational flexibility is seen in structural studies of covalently modified AChEs and in studies of ligand interactions at the peripheral anionic site and at the active site. As shall be developed in detail later (III. Reaction Dynamics), active site conformational flexibility is also an intrinsic feature of the induced-fit model for AChE catalytic power.

3. Hydrophobic Regions

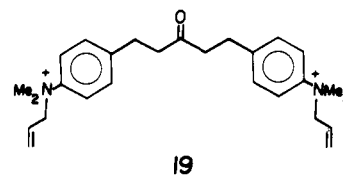
The discussions in the preceding section illustrate the capacity of the AChE active site for interaction with hydrophobic substrates and ligands. The anionic locus of the active site interacts with various classes of hydrophobic ligands: aromatic cations,^{2,3,25,33,105,109} bis-quaternary ammonium ligands (e.g. decamethonium, 3),^{2,3,100,103} *N*-alkyl quaternary ammonium ligands,^{2,25,100} and *N*-methylquinolinium substrates (e.g., 13).¹⁰⁹ The esteratic locus of the active site also interacts with hydrophobic substrates, such as 1-naphthyl acetate (15),^{2,109} indophenyl acetate (16),^{2,25,45} and tropolone acetate (17).³⁵



These substrate and ligand interactions are supported by structural studies of AChE that place hydrophobic residues at the active site. Shinitzky et al.¹¹³ characterized the interaction of *N*-methylacridinium (1) and *N*-benzylpyridinium (18) with AChE's active site. *N*-Benzylpyridinium binding was accompanied by quenching of tryptophan fluorescence of the enzyme. Binding of *N*-methylacridinium to AChE causes quenching of the ligand's fluorescence and appearance of a new absorption at ~ 470 nm. A similar *N*-methylacridinium absorption is observed in the presence of *N*-acetyl-L-tryptophan. Shinitzky et al.¹¹³ assign this new spectral feature to a charge-transfer complex between *N*-methylacridinium and a tryptophan residue in the AChE active site. The prominent charge-transfer band is consistent with face-to-face interaction, within ~ 5 Å, of the ligand with the active site tryptophan. Berman et al.¹¹⁴ also suggested the formation of a charge-transfer complex with tryptophan to explain differences in the absorption spectra of covalent (NBD-amino)ethyl and (NBD-amino)pentyl methylphosphono-AChE complexes (NBD = 7-nitrobenz-2-oxa-1,3-diazole). The absorption maxima and bandwidths were 475–480 nm and 3870 cm^{-1} , respectively, for the aminoethyl complex and 485–490 nm and 2870 cm^{-1} , respectively, for the aminopentyl complex. These results indicate that the NBD probe, which extends ~ 7 Å from the active site serine in the aminoethyl complex, makes a charge-transfer interaction (leading to band broadening and optical activity) with an active site tryptophan or tyrosine. The NBD probe of the aminopentyl complex extends ~ 12 Å from the active site serine and enjoys no such interaction. The spectral characteristics of pyrenebutyl methylphosphono-AChE are also consistent with a hydrophobic active site that contains tryptophan.⁷² In particular, the absorption spectrum of the pyrene moiety overlaps the emission of and quenches the fluorescence of enzyme tryptophans. The position of the long-wavelength absorption of the pyrene moiety in the covalent enzyme complex is 349 nm, which is red-shifted by 8 nm compared with pyrenebutanol in H_2O . This is consistent with binding of the pyrene moiety to a site on the enzyme that contains aromatic residues.

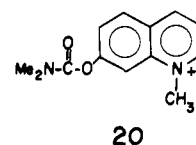
Majumdar and Balasubramanian⁷⁵ used various chemical modifications to characterize the active sites

for AChE-catalyzed hydrolysis of ACh, indophenyl acetate (16), and aryl amides. Types of residues essential for all three activities were lysine, tyrosine, tryptophan, and histidine. However, ACh and the competitive inhibitor 1,5-bis[4-(allyldimethylammonio)phenyl]pentan-3-one (19) afforded protection

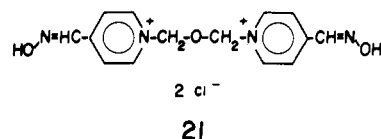


of ACh hydrolysis activity against inactivating reagents that modify the four amino acids above, but protect aryl amidase activity against modification of histidine and tyrosine only. Hence, the active site regions for ACh and indophenyl acetate hydrolyses on the one hand and for aryl amidase activity on the other are different, yet overlap, with a histidine and a tyrosine residue in common.

The presence of tyrosine in the active site is supported by inhibition of AChE by tetranitromethane (TNM) and arsenite,^{115,116} and perhaps by fluoride.^{117,118} Arsenite is a quasi-irreversible inhibitor because, though inhibition reaches equilibrium with a dissociation constant of $15\ \mu\text{M}$, breakdown of the enzyme-arsenite complex occurs slowly ($k = 1-2 \times 10^{-3}\text{ min}^{-1}$).¹¹⁶ Binding of arsenite to the enzyme is second order, with $k = 128\text{ M}^{-1}\text{ min}^{-1}$. Arsenite inhibits AChE-catalyzed hydrolysis of ATCh and indophenyl acetate (16) to the same extent and blocks carbamylation of the active site serine by the fluorescent ACh analogue *N*-methyl-7-dimethylcarbamoxymethylquinolinium iodide (M7C, 20).



Arsenite inhibition is completely blocked by *m*-(trimethylammonio)phenol and tensilon (11) and is partially blocked by tetramethylammonium. These ligands are thought to bind to the anionic locus of the active site.^{2,3,25} However, the quaternary pyridinium ligands 2-PAM (12), pyridine methiodide, and toxogonin (21)

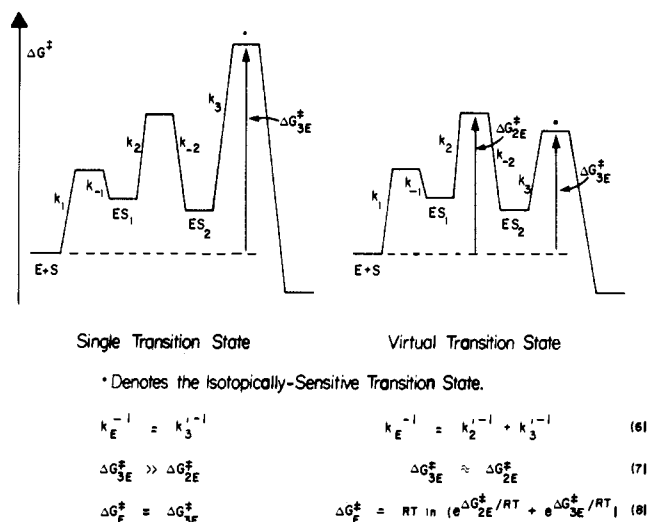


accelerate arsenite inhibition of AChE without affecting the dissociation constant of the enzyme-arsenite complex. TNM inhibits AChE by converting 12 of 21 tyrosine residues to 3-nitrotyrosines. Arsenite protects two tyrosines against TNM modification. Hence, Page and Wilson¹¹⁵ ascribe arsenite inhibition to formation of an arsenite diester with two active site tyrosines.

III. Reaction Dynamics

A. Introduction

As much of the discussion to this point illustrates, AChE is a conformationally plastic enzyme. This conformational plasticity includes the active site, as the

CHART VI. Comparative Activation Thermodynamics for Single and Virtual Transition States

wide-ranging substrate specificity of the enzyme demonstrates (cf. Table II). Whether active site conformational dynamics play a significant role in AChE catalytic function is a matter that can only be settled by experimental characterization of the anatomy of AChE catalysis (i.e., reaction dynamics and thermodynamics, intrinsic structural features of chemical transition states). Rosenberry^{2,27} earlier suggested that induced fit consequent to substrate binding is prominently rate limiting in the acylation stage of AChE catalysis. Quinn and Swanson¹⁸ determined pL-rate profiles (L = H, D) and measured solvent isotope effects in mixed H₂O–D₂O buffers for k_E of AChE-catalyzed hydrolysis of *o*-nitrochloroacetanilide (ONCA). They interpreted the isotope effects in terms of a virtual transition state that is comprised of contributions from transition states of serial microscopic physical and chemical steps. Because the mechanistic models offered by Quinn and Swanson¹⁸ and in consequent investigations^{19–21} of AChE from my laboratory rely heavily on the measurement of solvent isotope effects and the virtual transition-state concept, the requisite background is first presented.

B. The Virtual Transition-State Concept

1. Reaction Thermodynamics and Free Energy Diagrams

When a chemical reaction is rate limited by two or more microscopic transition states, whether they be of serial or parallel steps, the properties of the observed (phenomenological) transition state are weighted averages of the intrinsic structural features of the microscopic transition states that contribute to rate determination. In this situation the observed transition state is called a virtual transition state.^{10–12} The difference between a single rate-limiting and a virtual transition state in a linear three-step reaction sequence is illustrated by the free energy diagrams of Chart VI. Note that in the diagrams the ΔG^\ddagger values refer to the free enzyme and free substrate reactant state. If the enzyme is saturated by substrate (k_{ES} measurements), one may also have a virtual reactant state comprised of all kinetically significant ES complexes. In eq 6 of Chart VI $k_2' = k_1 k_2 / k_{-1}$ and $k_3' = k_1 k_2 k_3 / k_{-1} k_{-2}$ are the rate con-

stants for conversion of E + S to the k_2 and k_3 transition states, respectively. As the diagram shows, when the k_3 transition-state free energy is high ΔG_{3E}^\ddagger (and hence k_E) depends only on ΔG_{3E}^\ddagger . Transition-state structural features that are probed by isotope effects (for example) are in this case the intrinsic features of the k_3 transition state. When the observed transition state is a virtual transition state, ΔG_E^\ddagger contains both ΔG_{2E}^\ddagger and ΔG_{3E}^\ddagger , and the relative free energies of the k_2 and k_3 transition states determine their fractional contributions to the observed properties of the virtual transition state. This is illustrated by the transformations of eq 6 and 8 to eq 9 and 10. Eq 9 shows that k_2' and k_3' make frac-

$$k_E/k_2' + k_E/k_3' = f_2 + f_3 = 1 \quad (9)$$

$$e^{(\Delta G_{2E}^\ddagger - \Delta G_E^\ddagger)/RT} + e^{(\Delta G_{3E}^\ddagger - \Delta G_E^\ddagger)/RT} = 1 \quad (10)$$

tional contributions f_2 and f_3 , respectively, to rate determination. The fractional contributions (weighting factors) arise thermodynamically from ΔG_{2E}^\ddagger and ΔG_{3E}^\ddagger (eq 10). Since these quantities refer to the same initial state (E + S), the weighting factors are determined solely by the free energies of the k_2 and k_3 transition states.

Consider as an example a reaction for which $\Delta G_{2E}^\ddagger = \Delta G_{3E}^\ddagger$, the k_3 transition state is subject to a solvent isotope effect ($^{D_2}k_3 = 4$), and the k_2 transition state is isotopically insensitive ($^{D_2}k_2 = 1$). In this case $f_2 = f_3 = 0.5$ and the observed isotope effect is as shown in eq 11. Therefore, the observed transition state appears to

$$^{D_2}k_E = f_2 \cdot ^{D_2}k_2 + f_3 \cdot ^{D_2}k_3 = 2.5 \quad (11)$$

be rate limited by a proton transfer that gives an isotope effect of 2.5, but it is actually a virtual transition state in which an intrinsic isotope effect of 4 from the k_3 transition state is partially masked by equal rate determination by the k_2 transition state.

The reaction dynamics just described can be elaborated (eq 12 and 13) for reactions that involve m rate-determining transition-state contributors to the virtual transition state. Equation 13 is the general case of

$$f_1 + f_2 + \dots + f_m = 1 \quad (12)$$

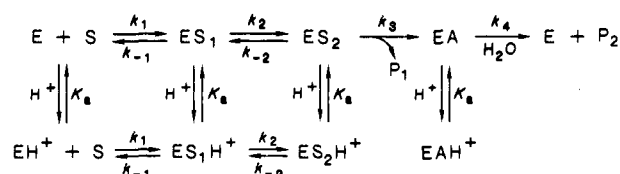
$$^X k_E = f_1 \cdot ^X k_1 + f_2 \cdot ^X k_2 + \dots + f_m \cdot ^X k_m \quad (13)$$

which eq 11 is a particular example, and it shows that a measured effect X on k_E (usually some isotope effect) arises from the successive intrinsic effects ($^X k_i$) on each of the transition states that contribute f_i to the virtual transition state. In any reaction, all microscopic transition states contribute to the virtual transition state, but in practice, only those transition states whose ΔG^\ddagger values are within ~ 2 kcal mol⁻¹ of the highest microscopic ΔG^\ddagger make important contributions.

2. Kinetic Equations

Scheme II presented an AChE mechanism that involved a kinetically significant induced-fit step (k_2). A more general form of this mechanism as a function of pH is given in Scheme VI. Definitions of terms in Scheme VI were presented in Scheme II. Scheme VI assumes that a single pK_a describes the acid–base behavior of all forms of the enzyme. Furthermore, the pK_a on which activity depends is assumed to be ~ 6.3 , which has long been assigned to the active site histidine.^{2,25} These assumptions are justified for a number of reasons:

SCHEME VI



(1) k_{ES} for AChE-catalyzed hydrolysis of ACh and phenyl acetate (both of which involve predominantly rate-determining deacetylation^{26,27}) depends on the basic form of an active site amino acid with $pK_a = 6.5$.²⁷ (2) k_{ES} for AChE-catalyzed hydrolysis of *o*-nitrophenyl acetate depends on a $pK_a = 6.3$.¹⁹ This reaction is probably partially rate limited by both acylation (k_3) and deacylation (k_4). (3) The acylation rate constant k_E depends on a $pK_a \sim 6.3$ for cationic substrates of AChE.^{2,27,76} Though this effect may arise from the pH dependence of the k_3 component of k_E , it is also likely that cationic substrates do not bind appreciably to the protonated form of the free enzyme (EH^+), since cationic inhibitor binding decreases with a $pK_a \sim 6.3$.^{2,76,77} (4) Though k_E for neutral substrates frequently depends on pK_a values of 5.2–5.8,^{2,18–20,27} for poorly reactive substrates the pK_a approaches 6.3.²⁷ Since the reactant state for k_E measurements is $E + S$, pK_a values determined from pH- k_E profiles *must* be those of the free enzyme. As shall be seen later, the low pK_a values for reactive neutral substrates of AChE can be rationalized in terms of prominent rate determination by a microscopic component of k_E that is pH insensitive.^{2,18–20,27} (5) Krupka interpreted the pH dependence of betaine binding in terms of the conversion of a cationic to a neutral amino acid with a $pK_a = 6.3$.⁷⁶ This behavior is consistent with titration of an imidazolium residue but not of a neutral carboxyl. (6) Reagents that acylate the imidazole side chain of histidine, such as ethoxyformic anhydride⁷⁴ and diethylpyrocarbonate,⁷⁵ inhibit AChE. Inhibition can be reversed with hydroxylamine and blocked by substrate and competitive inhibitors.

A steady-state derivation of the phenomenological kinetic parameters for Scheme VI gives eq 14 and 15.

$$k_E = \frac{k_3'K_a}{[H^+] + K_a(1 + C)} \quad (14)$$

$$k_{ES} = k_2k_3k_4/[k_4\{k_{-2}(1 + [H^+]/K_a) + k_3\} + k_2(k_3 + k_4)(1 + [H^+]/K_a)] \quad (15)$$

Equation 15 reduces to eq 1 and eq 14 to eq 3 (vide supra) when $[H^+] \ll K_a$. The commitment to chemical catalysis, C , was also defined earlier. C has two limiting forms. For highly reactive substrates, k_E is likely prominently rate limited by binding (i.e., $k_{-1} \ll k_2$) and $C = k_3/k_{-1}K_2$, where $K_2 = k_{-2}/k_2$. In this case, C measures the tendency of ES_2 to proceed to EA , vs. reversion to $E + S$ via the kinetically significant k_{-1} transition state. For less reactive substrates, $C = k_3/k_{-2}$ and measures a similar partitioning of ES_2 , albeit with reversion to $E + S$ via the kinetically significant k_{-2} transition state. Hence, C is a measure of the reaction dynamics and thermodynamics of the acylation stage of AChE catalysis. How C is determined is discussed later. Equation 15 reduces to eq 16 when the rate-determining step at substrate saturation is acylation (i.e., when $k_4 \gg k_3$ and k_2). Equations 14–16 will prove

$$k_{ES} = \frac{k_2k_3}{(k_{-2} + k_2)(1 + [H^+]/K_a) + k_3} \quad (16)$$

useful in the following sections of this review in accounting for solvent isotope effects and pH-rate profiles for AChE-catalyzed reactions of neutral substrates.

3. Kinetic Solvent Isotope Effects: Predictions

A prominent methodology for characterizing transition-state structures for hydrolytic enzymes is the measurement of solvent isotope effects.^{119–121} Solvent isotope effects on the phenomenological kinetic parameters are defined in eq 17. Rate constants with the

$${}^{D_2O}k_E = k_E^{H_2O}/k_E^{D_2O} \quad {}^{D_2O}k_{ES} = k_{ES}^{H_2O}/k_{ES}^{D_2O} \quad (17)$$

superscripts following correspond to measurements in the respective isotopic solvents. Prototropic catalysis, such as general acid–base catalysis or H bonding, is a common transition-state structural feature of hydrolytic reactions. Many of the functionalities of enzymes that are involved in prototropic catalysis (e.g., ROH, RCO₂H, RSH, RR'NH) exchange protons very rapidly with solvent,^{119–121} so that reactions in D₂O proceed with deuteriotropic catalysis. For organic reactions, ${}^{D_2O}k$ values of 1.5–4 are typical and are indicative of rate-determining transition states that are stabilized by proton transfers.

The proton inventory technique produces additional resolution of transition-state structural features from solvent isotope effect measurements. Some salient features of this technique are described herein. For broader coverage, the reader is referred to several reviews that have appeared in recent years.^{119–121} In a proton inventory experiment rates or rate constants are measured in a series of mixtures of equivalent H₂O and D₂O buffers. Equivalent buffers are those for which concentrations of buffer components, electrolytes, etc. are the same. The dependence of a rate constant k_n on the atom fraction n of deuterium in mixed isotopic buffers is given by the Gross–Butler equation (eq 18).

$$k_n = k_0 \frac{\prod_j (1 - n + n\phi_j^T)}{\prod_i (1 - n + n\phi_i^R)} \quad (18)$$

The numerator of eq 18 contains a product of terms for each transition-state proton that makes a contribution $1/\phi_j^T$ to the observed solvent isotope effect; ϕ^T is the transition-state fractionation factor. The denominator contains a similar product of terms for readily exchangeable protons of the reactant state. The rate constant k_0 is that in H₂O ($n = 0$). Though enzyme reactions involve a large number of protons, several features simplify the picture considerably: (1) Only those protons for which $\phi \neq 1$ contribute to the solvent isotope effect. (2) Only those protons whose fractionation factors change on activation (i.e., $\phi_i^R \neq \phi_j^T$; $i = j$) contribute to the solvent isotope effect. In addition, processes that may be subject to solvent isotope effects that arise from cumulative small isotope effects from numerous protons (e.g., enzyme conformational change, desolvation that accompanies substrate binding) can be readily modeled, as discussed below.

There are several special cases of eq 18 that deserve comment. For many amino acid functionalities involved in prototropic catalysis, such as ROH, RCO₂H,

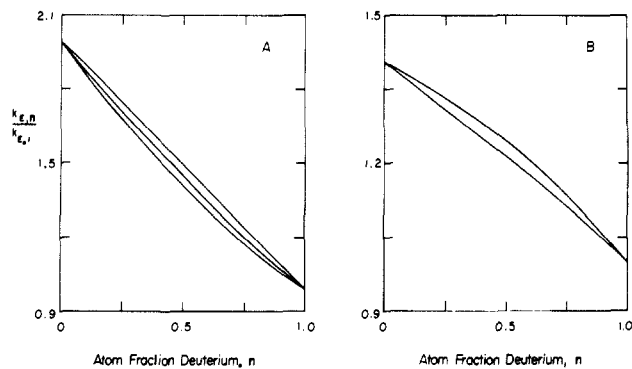


Figure 1. A. Computer-simulated proton inventories for reactions that are subject to $D_2O k_E = 2$ that arises from one-proton catalysis (top line), two-proton catalysis (middle line), or many-proton catalysis (bottom line). B. Computer-simulated proton inventories for reactions that are rate limited by virtual transition states that are comprised of serial microscopic transition states for k_2 and k_3 that make fractional contributions to rate determination of $f_2 = 0.67$ and $f_3 = 0.33$, respectively. Top line: $D_2O k_2 = 1$, $D_2O k_3 = 2.2$. Bottom line: $D_2O k_2 = 1.2$, $D_2O k_3 = 1.8$.

and $RR'NH$, $\phi^R \cong 1$; an exception is RSH , for which $\phi^R = 0.4$ – 0.6 .^{119–123} However, cysteine is not involved in AChE catalysis, since thiol-modifying reagents do not affect activity.^{2,116} *E. electricus* AChE contains no free sulfhydryl groups,² while the *T. californica* AChE contains only one, that of Cys^{231,65}. Therefore, for AChE eq 18 reduces to a polynomial function of n as shown in eq 19. If a single proton contributes to the solvent

$$k_a = k_0 \prod_j (1 - n + n\phi_j^T) \quad (19)$$

isotope effect, a plot of k_n vs. n will be best described by a straight line. If two or more protons contribute to the solvent isotope effect, the dependence of k_n on n is described by a quadratic or higher order polynomial and will be curvilinear and downward bowing. The predicted proton inventory when a large number of fractionating protons contribute to the solvent isotope effect is particularly interesting. This might be the situation for a kinetically significant enzyme isomerization or for desolvation of substrate and enzyme active site on substrate binding. Consider a case wherein $D_2O k = 2$ arises from a large number ν of proton sites with an average ϕ^T slightly < 1 :

$$k_n = k_0 [1 - n(1 - \phi^T)]^\nu \quad (20)$$

After rearranging and taking the logarithm transform of eq 20 one gets

$$\ln(k_n/k_0) = \nu \ln[1 - n(1 - \phi^T)] \sim \nu n(1 - \phi^T) \quad (21)$$

Since $1 - \phi^T$ is almost 0, $\ln[1 - n(1 - \phi^T)] \sim n(1 - \phi^T)$, which accounts for the final form of the right hand side of eq 21. Similarly, when $n = 1$, $\ln(k_1/k_0) = \nu(1 - \phi^T)$. Therefore:

$$\ln(k_n/k_0) = n \ln(k_1/k_0) \quad (22)$$

Taking antilogs and rearranging gives eq 23. Equation

$$k_n = k_0 Z^{-n}, \text{ where } Z = k_0/k_1 \quad (23)$$

23 predicts an exponential dependence of k_n on n . Computer-generated plots for a reaction that is subject to $D_2O k$ that arises from one- or two-proton catalysis (eq 19) or many-proton catalysis (eq 23) are shown in Figure 1A. As expected, the curvature of the proton inventory

increases as the number of fractionating transition-state protons increases. With rate constants of 1–2% precision, one can generally distinguish among one-, two-, and many-proton catalysis.¹¹⁹

A mechanistic model that is particularly germane to AChE catalysis is one in which two microscopic steps contribute to rate determination (i.e., the virtual transition-state model). Consider a case in which k_E (acylation) is rate limited by k_2 and k_3 of Scheme II and VI. In this case, at $pH \gg pK_a$ eq 14 reduces to eq 6 (cf. Chart VI). For the moment, assume that only k_3 is subject to a solvent isotope effect ($D_2O k_3$), which arises from a transition state that is stabilized by simple general acid–base (one-proton) catalysis. The requisite Gross–Butler equation that comes from eq 6 for this model is

$$1/k_{E,n} = 1/k_2' + 1/k_3'(1 - n + n\phi_3^T) \quad (24)$$

The rate constants k_2' and k_3' were defined in Chart VI and the corresponding text; $\phi_3^T (= 1/D_2O k_3)$ is the fractionation factor of the general acid–base proton bridge that stabilizes the k_3 transition state. This equation is converted to a more useful form by multiplying and dividing the right hand side by k_E :

$$k_{E,n}^{-1} = k_E^{-1} \left(f_2 + \frac{f_3}{1 - n + n\phi_3^T} \right) \quad (25)$$

Equation 25 predicts a rational functional dependence of $k_{E,n}$ on n ; f_2 and f_3 are the respective fractional rate determinations of the k_2 and k_3 transition states:

$$f_2 = \frac{k_E}{k_2'} = \frac{k_3'}{k_2' + k_3'} \quad f_3 = \frac{k_E}{k_3'} = \frac{k_2'}{k_2' + k_3'} \quad (26)$$

Figure 1B shows a computer-simulated proton inventory, plotted as partial solvent isotope effects $k_{E,n}/k_{E,1}$, generated from eq 25 for a reaction that has an observed isotope effect $D_2O k_E = 1.4$ that arises from a 33% rate-determining k_3 transition state for which $D_2O k_3 = 2.2$. A similar proton inventory simulation has been described by Kovach et al.²² As the plot illustrates, the virtual transition-state model produces a proton inventory plot that is strongly curvilinear and upward bowing. If the k_2 transition state produces even a modest isotope effect (e.g., $D_2O k_2 = 1.2$), the curvature of the proton inventory is greatly reduced (cf. Figure 1B).

The relationship of the observed and intrinsic isotope effects can be generated from eq 25 with $n = 1$ as shown in eq 27. Equation 27 is a particular case of eq 11 and

$$D_2O k_E = f_2 + f_3 D_2O k_3 \quad (27)$$

13 that were presented earlier. If one inserts the rate constant ratios of eq 26 for the f values, eq 28 results.

$$D_2O k_E = \frac{D_2O k_3 + C}{1 + C}, \text{ where } C = k_3/k_2 \quad (28)$$

This equation is that which comes from the oft-used approach to enzyme kinetics of the Wisconsin enzymologists (et al.), as originally developed by Northrop.^{23,24} Therefore, though the terminology and methods of the virtual transition-state and Northrop approaches appear different, the two ways of analyzing enzymic isotopic effects are equivalent. The relation-

TABLE V. Kinetic Parameters and Isotope Effects for AChE-Catalyzed Hydrolysis of Anilides and Esters^a

substrate	$10^{-3} k_E, M^{-1} s^{-1}$	k_{ES}, s^{-1}	$D_2O k_E$	$D_2O k_{ES}$	$D k_E^b$	$D k_{ES}^b$
ACh ^c	1.6×10^5	16 000	1.1 (± 0.1)	2.3 (± 0.2)	0.99 (± 0.04) ^h	
ONPA ^d	7690	2000	1.2 (± 0.2)	2.4 (± 0.4)		
PA ^e	7900	17 100	1.07 (± 0.03)	1.89 (± 0.06)	1.002 (± 0.026)	0.961 (± 0.017)
			1.2 (± 0.2)	2.0 (± 0.3)		
PA ^d	1915	2720	1.5 (± 0.1)	2.3 (± 0.2)		
			1.33 (± 0.02)	2.26 (± 0.06)		
PA ^e	9900	24 000	1.16 (± 0.08)	1.46 (± 0.07)		
			1.6 (± 0.1)	2.42 (± 0.03)		
PMPF ^f	3100	6260	1.09 (± 0.01)	2.65 (± 0.10)	0.99 (± 0.01)	0.93 (± 0.02)
PCA ^d	2180	370	1.0 (± 0.1)	1.81 (± 0.04)		
PMPCA ^d	250	200	0.93 (± 0.02)	1.6 (± 0.1)		
PNPA ^g	22.4		1.56		0.99 (± 0.02) ^h	
	251		1.93 (± 0.07)			
ONCA ^f	103	82	1.31 (± 0.02)	1.75 (± 0.03)	1.02 (± 0.02)	
ONA ^f	7.8	156	1.55 (± 0.03)		0.982 (± 0.005)	
ONFA ^f	1.94	4.1	1.41 (± 0.03)	1.85 (± 0.09)	0.88 (± 0.02)	0.85 (± 0.06)
methyl acetate ^f	1.3		2		1.10 (± 0.06) ^h	

^a All reactions were conducted at 25 °C save those for PCA and PMPCA, which were conducted at 20 °C. ^b Secondary isotope effects for ACh, ONPA, PNPA, and methyl acetate are β -D effects; those for PMPF and ONFA are α -D effects. ^c Data are from ref 27. ^d Data are from ref 19. ^e Data are from ref 22. The first row of isotope effects is for catalysis by *E. electricus* AChE. The second row of isotope effects is for reactions catalyzed by human erythrocyte AChE. ^f ONFA, *o*-nitroformanilide; data are from ref 20. ^g The first row of data for PNPA is from ref 43; k_E was calculated from specified mass of partially pure enzyme and should therefore be taken as a lower limit. The second row of data is from ref 27. ^h β -D effects for ACh, PNPA, and methyl acetate are from ref 43.

ship of the commitment of ES₂ to chemical catalysis and the weighting factors of the k_2 and k_3 transition states is that of eq 29.

$$f_2 = \frac{C}{C+1} \quad f_3 = \frac{1}{C+1} \quad (29)$$

The virtual transition-state model provides an interpretive framework for illuminating transition-state structural features and reaction dynamics for the acylation stage of AChE catalysis. In addition, various AChE reactions give proton inventories that are consistent with simple general acid-base (one-proton) catalysis.^{19,21,22} The use of the solvent isotope effect and proton inventory probes to characterize several AChE-catalyzed reactions is presented later.

4. pH-Rate Profiles

The virtual transition-state description of AChE reaction dynamics has important implications for the pH- k_E behavior of the enzyme if the isotopically insensitive k_2 transition state is also pH insensitive, as the Scheme VI mechanism shows.^{2,18,20,27} In this situation, the dependence of k_E on pH is given by eq 14, from which one can derive the relationship^{2,18,20} shown in eq 30 of the observed pK_a for k_E and the intrinsic pK_a for the k_3 step. Hence, as $C = k_3/k_{-2}$ gets larger and the $pK_a(\text{observed}) = pK_a(\text{intrinsic}) - \log(1 + C)$ (30)

k_2 transition state is correspondingly increasingly rate determining, the observed pK_a increasingly underestimates the intrinsic pK_a . Since $C = f_2/f_3$ (cf. eq 29) and the weighting factors can be determined from proton inventory experiments (cf. eq 25), the intrinsic pK_a can be calculated from eq 30.

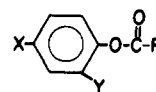
C. Virtual Transition States for Anilide Hydrolyses

1. Probes of Virtual Transition States for k_E

a. Solvent Isotope Effects. As discussed earlier, k_E for AChE-catalyzed hydrolysis of ACh^{2,30} (and of

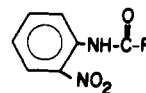
CHART VII. Aryl Ester and Anilide Substrates of AChE (L = H, D)

Esters



- X = MeO, Y = H, R = L *p*-methoxyphenyl formate (PMPF)
 X = H, Y = NO₂, R = CL₃ *o*-nitrophenyl acetate (ONPA)
 X = Y = H, R = CH₃ phenyl acetate (PA)
 X = MeO, Y = H, R = CH₂Cl *p*-methoxyphenyl chloroacetate (PMPCA)
 X = Y = H, R = CH₂Cl phenyl chloroacetate (PCA)

Anilides



- R = L *o*-nitroformanilide
 R = CL₃ *o*-nitroacetanilide (ONA)
 R = CL₂Cl *o*-nitrochloroacetanilide (ONCA)

ATCh^{31,33}) is diffusion controlled. Though this attests to the catalytic power of the enzyme, diffusion control masks all transition states in the acylation stage of catalysis save that of the chemically uninformative k_1 step. Fortunately, the wide AChE substrate specificity allows one to circumvent this problem by using a number of structurally related substrates that span a wide range of reactivity. One might expect that as k_E decreases in such a series of substrates the chemical transition state k_3 will become increasingly rate determining. Accordingly, co-workers in my laboratory have synthesized the substrates shown in Chart VII. The kinetic parameters for these substrates and for phenyl acetate (PA) are given in Table V, along with isotope effects that were measured in other laboratories.

Two features of the data in Table V are noteworthy: (1) The substrates span a range of k_E of five orders of magnitude. Since k_E is $>10^6 M^{-1} s^{-1}$ for the more re-

TABLE VI. Calculated Intrinsic Parameters for AChE-Catalyzed Hydrolysis of Anilides and Aryl Esters

substrate	$D_2O k_3$	f_2	f_3	C	observed pK_a	intrinsic pK_a
ONCA ^a	2.3 (± 0.2) 1.94 (± 0.04) ^b	0.67 (± 0.06)	0.33 (± 0.06)	2.0 (± 0.4)	5.80 (± 0.03)	6.28 (± 0.09)
ONA ^a	2.5 (± 0.2) 1.92 (± 0.02) ^b	0.58 (± 0.05)	0.42 (± 0.05)	1.4 (± 0.2)	5.63 (± 0.03)	6.00 (± 0.09)
ONFA ^a	2.3 (± 0.3)	0.67 (± 0.06)	0.33 (± 0.06)	2.0 (± 0.4)	5.62 (± 0.04)	6.1 (± 0.1)
PNPA ^c	2.39 (± 0.08)	0.61 (± 0.02)	0.39 (± 0.02)	1.6 (± 0.1)	5.6 (± 0.1)	~6.6
PMPF ^a	~2	~0.9	~0.09	~10		

^a Except where indicated, data are from ref 20. Data for PMPF are estimates (save the observed pK_a); see text for elaboration. ^b Solvent isotope effects were calculated from the linear-least-squares fits of Figure 6, as detailed in ref 21. ^c Reference 43.

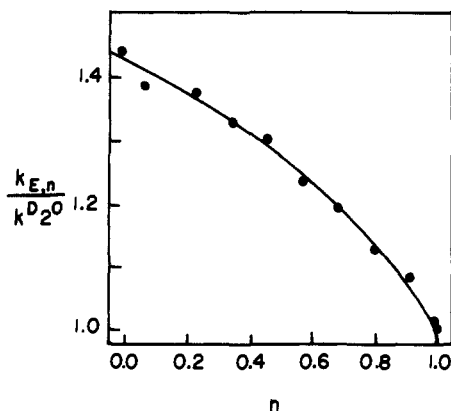


Figure 2. Proton inventory for k_E of AChE-catalyzed hydrolysis of ONCA. Reproduced with permission from ref 18. Copyright 1984, American Chemical Society.

active ester substrates, it is conceivable that binding (k_1) is at least partially rate determining. However, k_E is much smaller for anilides that are nearly isosteric with aryl esters (compare ONA and ONPA), so that microscopic events after binding of these substrates must be rate determining. (2) As k_E decreases, $D_2O k_E$ values tend to increase. Except for PA, the reactive ester substrates (ACh through PMPA) have an average $D_2O k_E$ of 1.06 ± 0.09 . Less reactive substrates (anilides, PNPA, methyl acetate) give moderate normal $D_2O k_E$ values. Therefore, decreasing substrate reactivity is accompanied by partial exposure to rate determination of the chemical k_3 transition state. This conclusion is supported by the trend in substrate secondary isotope effects $D k_E$ (cf. Table V), which is consistent with increasing expression of nucleophilic enzyme-substrate interaction in the virtual transition state with decreasing reactivity.

The considerations raised in the preceding paragraph indicate that for anilide substrates the k_2 and k_3 transition states both contribute to rate determination for k_E . This conclusion is supported by nonlinear, upward-bulging proton inventories for ONCA,¹⁸ ONA, and ONFA,²⁰ the ONCA proton inventory is shown in Figure 2. Anilide proton inventories were fit by nonlinear least squares to eq 25,¹²⁴ with k_E , f_3 and ϕ_3^T as adjustable parameters. Results of these analyses are contained in Table VI, and show that the small $D_2O k_E$ values of Table V arise from intrinsic isotope effects of ~ 2 for k_3 transition states that are 30–45% rate determining. The $D_2O k_3$ values are similar to solvent isotope effects for k_{ES} of AChE reactions (cf. Table V).^{19,21,22,27} Hogg et al.⁴³ reported a nonlinear, upward-bulging proton inventory for k_E of AChE-catalyzed hydrolysis of *p*-nitrophenyl acetate (PNPA), which they interpreted in terms of a transition-state contribution to the solvent isotope effect of 2.2 (i.e., $\phi^T = 0.45$) that is offset by an

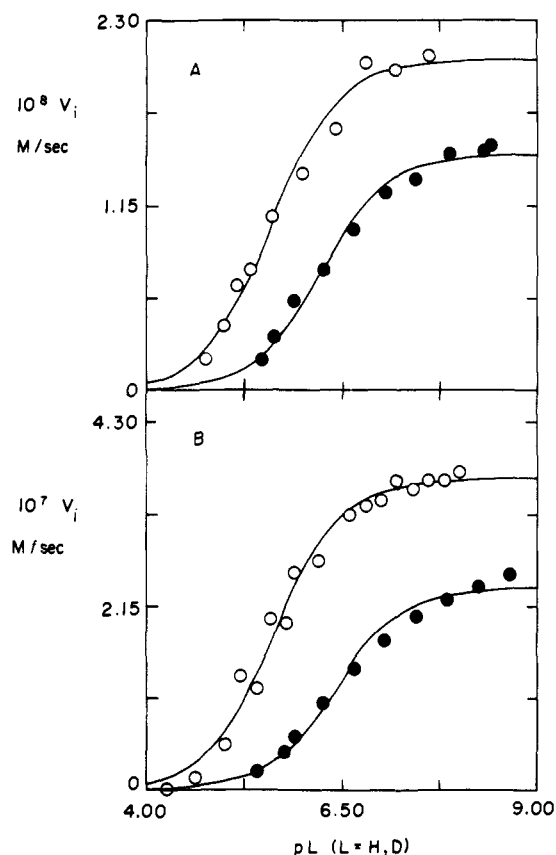


Figure 3. pL-Rate profiles ($L = H, D$) for AChE-catalyzed hydrolysis of ONFA (A) and ONA (B). Reproduced with permission from ref 20. Copyright 1987, American Chemical Society. Initial velocities (V_i 's) were measured at $[S]_0 \ll K_m$. Open circles are V_i 's measured in H_2O buffers, and closed circles are V_i 's measured in D_2O buffers.

inverse isotope effect of 0.7 from a reactant-state proton (i.e., $\phi^R = 0.7$). However, their proton inventory is also accommodated by the virtual transition-state model discussed herein. As the results in Table VI for least-squares analysis of their proton inventory show, PNPA is rate limited by a virtual transition state wherein the intrinsic isotope effect and weighting factors for k_2 and k_3 are similar to those for the anilide substrates. It is not surprising that the $D_2O k_3$ for PNPA is partially expressed in $D_2O k_E$, since the reactivity of this ester is about the same as that of ONCA (cf. Table V).

The pL- k_E profiles ($L = H, D$) for ONFA and ONA in Figure 3 show that activity depends on the basic form of a single titratable amino acid side chain of the free enzyme, as described by eq 31. The observed pK_a

$$k_{E,pL} = \frac{k_E K_a}{[L^+] + K_a} \quad (31)$$

values given in Table VI were calculated by nonlin-

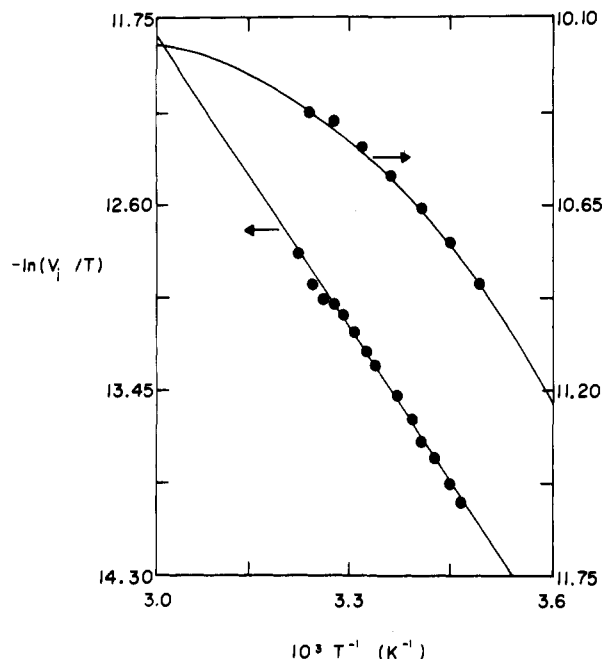


Figure 4. Eyring plots for AChE-catalyzed hydrolysis of ONCA. Reproduced with permission from ref 21. Copyright 1987, American Chemical Society. The upper plot was constructed from first-order rate constants that were determined at $[\text{ONCA}]_0 = K_m/20$ in 0.1 M sodium phosphate buffer that contained 0.1 N NaCl. The lower plot was constructed from initial velocities that were measured at $[\text{ONCA}]_0 \ll K_m$ in the same buffer that also contained 1% DMSO, v/v .

ear-least-squares fits of the respective $\text{pH}-k_E$ profiles to eq 31. Like the reactive esters studied by Rosenberry,²⁷ the anilides have $\text{p}K_a$ values that are well below the intrinsic $\text{p}K_a = 6.3^{22,25,76,77}$ of the active site histidine. Low $\text{p}K_a$ values have also been measured for inhibition of AChE by neutral carbamylating reagents.⁷⁸ These inhibitions are analogous to the acylation stage of catalysis. The intrinsic $\text{p}K_a$ for k_E of each anilide was calculated by using eq 30 and the requisite values of observed $\text{p}K_a$ and C in Table VI. These intrinsic $\text{p}K_a$ values are also given in the table and fall in the range 6.0–6.3, which is in good agreement with the intrinsic $\text{p}K_a$ of the AChE active site.

The Eyring plots¹²⁵ for k_E of AChE-catalyzed hydrolyses of PMPF, ONCA, ONA, and ONFA are nonlinear and bulge upward (Figure 4).²⁰ This type of dependence is probably not a temperature effect on the stability of AChE, since the Eyring plot for k_{ES} of PMPF hydrolysis is linear. A reasonable explanation for the temperature dependence of k_E for anilides can be constructed from eq 6 of Chart VI. Equation 32 is derived from the form of eq 6 for the virtual transition state by using the Eyring equation,¹²⁵ $k = (k_B T/h)e^{-\Delta G^\ddagger/RT}$. In this equation $A = (h/k_B)e^{-\Delta S_{3E}^\ddagger/R}$ and B

$$-\ln(k_E/T) = \ln(Ae^{\Delta H_{3E}^\ddagger/RT} + Be^{\Delta H_{3E}^\ddagger/RT}) \quad (32)$$

has the same form for ΔS_{3E}^\ddagger . The curvilinear Eyring plot of Figure 4 was fit to eq 32.

The model that was used to generate the curvilinear fits for anilide proton inventories (cf. eq 25) assumes that the k_3 transition state is stabilized by a single-proton transfer. The linear proton inventories for k_{ES} of ester hydrolyses^{19,22} support this assumption (vide infra). Furthermore, AChE-catalyzed hydrolyses of ONCA and ONA are inhibited by DMSO.²¹ Inhibition

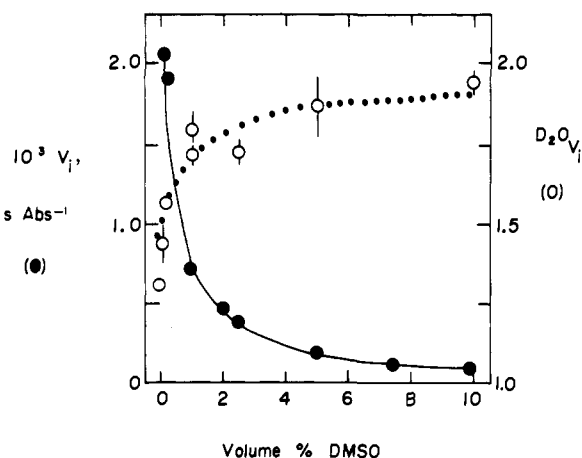


Figure 5. Effect of DMSO on initial velocities (V_i 's) and solvent isotope effects ($^{D_2O}V_i$'s) for AChE-catalyzed hydrolysis of ONCA. Reproduced with permission from ref 21. Copyright 1987 American Chemical Society. All initial velocity measurements were done at $[\text{ONCA}]_0 \ll K_m$.

of ONCA hydrolysis is competitive in form. However, DMSO has a more significant effect than simply competing with substrate for binding to the free enzyme. As Figure 5 shows, increasing DMSO inhibition of ONCA hydrolysis is accompanied by increasing expression of $^{D_2O}k_3$. These observations indicate that DMSO effects a change in rate-determining step that exposes the k_3 transition state. The data of Figure 5 for DMSO inhibition were fit to eq 33 by nonlinear least squares. For the fit in Figure 5, $K_i = 0.38 \pm 0.08\%$

$$V_i = V_i^0 / (1 + [I]/K_i) \quad (33)$$

v/v . This value was used as a constrained parameter, and the solvent isotope effects of Figure 5 were fit to eq 34. This equation comes from eq 28 and ascribes

$$^{D_2O}k_E = \frac{^{D_2O}k_3 + C/(1 + [I]/K_i)}{1 + C/(1 + [I]/K_i)} \quad (34)$$

the effect of DMSO on $^{D_2O}k_E$ to progressive decrease of the commitment to catalysis as $[\text{DMSO}]$ increases. The fit of the solvent isotope effects in Figure 5 gives $^{D_2O}k_3 = 1.95 \pm 0.05$ and $C = 1.1 \pm 0.3$. Though somewhat different than the values for ONCA in Table VI, these results yet support the assignment of a virtual transition state for k_E . Moreover, one predicts from eq 34 that at high $[\text{DMSO}]$ $^{D_2O}k_E = ^{D_2O}k_3$; i.e., the k_3 transition state is solely rate determining and the intrinsic isotope effect is unmasked. If the k_3 transition state is solely rate limiting, Eyring plots and proton inventories should be linear. As Figures 4 and 6 show, this is precisely what happens for AChE-catalyzed hydrolysis of ONCA and ONA. The linear proton inventories of Figure 6 provide additional support for the assumption inherent in eq 25 that AChE stabilizes the k_3 transition state by one-proton catalysis. The $^{D_2O}k_3$ values for DMSO-inhibited AChE-catalyzed hydrolysis of ONCA and ONA are included in Table VI.

b. Substrate Secondary Isotope Effects. The substrate secondary isotope effects of Table V also indicate that the chemical transition state k_3 is increasingly rate determining as k_E decreases. Consider the α -deuterium secondary isotope effect for ONFA, $^{D}k_E = 0.88 \pm 0.02$. The expected effect for equilibrium for-

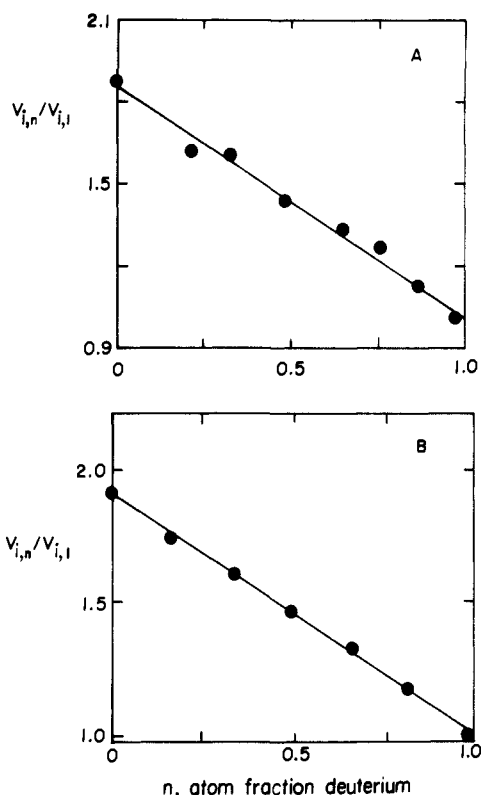


Figure 6. Proton inventories for DMSO-inhibited AChE-catalyzed hydrolysis of ONCA (A) and ONA (B). Reproduced with permission from ref 21. Copyright 1987 American Chemical Society.

mation of a tetrahedral intermediate in the acylation stage of catalysis is $^Dk \sim 0.7^{126-128}$ and is thought to arise primarily from conversion of the low frequency out-of-plane bending mode of the formyl function ($\sim 800 \text{ cm}^{-1}$) to a higher frequency bending mode ($\sim 1350 \text{ cm}^{-1}$) in the tetrahedral intermediate.¹²⁹ In addition, the α -D effect depends nearly linearly on the degree of conversion in the transition state to sp^3 hybridization of the sp^2 -hybridized carbonyl carbon of substrate.¹²⁸ If the α -D effect dependent step for k_E of ONFA hydrolysis is the k_3 step, the intrinsic isotope effect can be calculated from eq 35. The calculated intrinsic

$$^Dk_E = \frac{^Dk_3 + C}{1 + C} \quad (35)$$

effect is $^Dk_3 = 0.64 \pm 0.10$, which is consistent with a k_3 transition state that closely resembles the tetrahedral intermediate. The β -D secondary isotope effect $^Dk_E = 0.982 \pm 0.005$ for ONA hydrolysis is also consistent with nucleophilic enzyme-substrate interaction. The expected effect for equilibrium conversion of the substrate to a tetrahedral intermediate is inverse by $4.6 \pm 0.6\%$ per D.¹³⁰ Hence, the effect for ONA of $0.6 \pm 0.2\%$ per D is consistent with a modest degree of nucleophilic enzyme-substrate interaction in the virtual transition state. However, the ONA secondary isotope effect and the other β -D effects in Table V are complicated by the fact that partition coefficients of carbonyl compounds for phase transfer from H_2O to hydrophobic organic solvents are subject to normal (i.e., >1) β -D effects of 1–2% per D.¹³¹ This kind of phase-transfer β -D effect may operate for k_E of AChE-catalyzed reactions, especially since the active site is hydrophobic (vida supra: II. AChE Structure).

2. Consideration of Alternate Models

There are four alternate models that accommodate the nonlinear and upward-bulging proton inventories for anilides and PNPA. The first model is one in which a normal isotope effect contribution from a transition-state proton bridge is partially offset by a reactant-state proton that has $\phi^R < 1$. This is the explanation offered by Hogg et al.⁴³ for the bowing-upward proton inventory for k_E of AChE-catalyzed hydrolysis of PNPA. The Gross-Butler equation for this model is given in eq 36.

$$k_{E,n} = k_E \frac{1 - n + n\phi^T}{1 - n + n\phi^R} \quad (36)$$

A fit that is indistinguishable from that of Figure 2 for AChE-catalyzed hydrolysis of ONCA can be generated from eq 36 with $\phi^T = 0.44$ and $\phi^R = 0.62$. The weakness of this model is the isotopic insensitivity of k_E for esters that span several orders of k_E reactivity (compare ACh, ONPA, PMPF, PCA, and PMPCA in Table V), which requires a fortuitous cancellation of ϕ^T and ϕ^R . Unlike the virtual transition-state model, the model embodied in eq 36 does not accommodate the pH- k_E behavior and nonlinear Eyring plots for AChE-catalyzed hydrolysis of neutral substrates. In addition, there are no prototropic amino acid side chains in *E. electricus* AChE that are expected to have a $\phi^R = 0.62$. Of the common organic functionalities, only RSH has $\phi^R < 1$,¹¹⁹⁻¹²³ but the enzyme is devoid of cysteine.² Only the short, strong H bonds described by Kreevoy et al.¹³² if present in AChE, are capable of generating the ϕ^R required by this model.

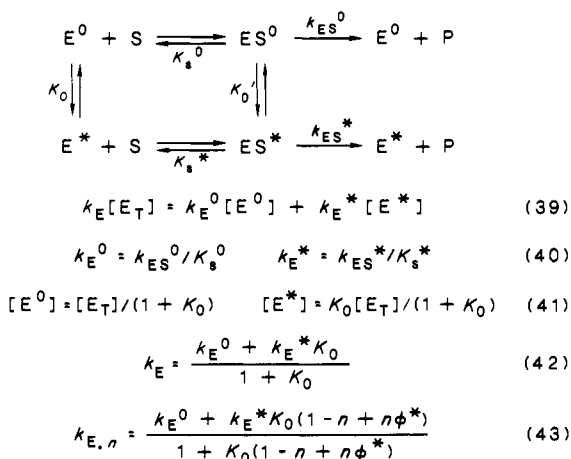
A second model that generates upward-bowing proton inventories is one in which k_3 is solely rate determining, but in which the substrate binding component k_1/k_{-1} of k_E is subject to an inverse solvent isotope effect that arises from many-proton fractionation (i.e., a Z term; vid supra, eq 23). Binding solvent isotope effects, which likely arise from partial desolvation of substrate and enzyme active site, have been postulated by Stein¹⁵⁻¹⁷ for k_E of elastase-catalyzed reactions. Equation 37 corresponds to this model. This equation

$$k_{E,n} = k_E Z^{-n} (1 - n + n\phi_3^T) \quad (37)$$

produces a fit that is indistinguishable from that of Figure 2 when $Z = 0.71$ and $\phi_3^T = 0.5$. The weakness of the model embodied in eq 37 is again the isotopic insensitivity of k_E for esters (cf. Table V). If binding is primarily rate determining, which is possible for the more reactive esters, one should observe $^D_2O k_E \sim Z$. The absence of solvent isotope effects for esters requires in each case the fortuitous cancellation of the isotope effect generated by the Z term. Such a situation strains credulity. In addition, this model does not provide a rationale for the low pK_a values for k_E .

A third model that can generate upward-bowing proton inventories is a particular case of the virtual transition-state model of eq 25, wherein the isotope effect from a one-proton k_3 transition state is offset by a many-proton isotope effect for the k_2 step. This situation is described by eq 38. This model accounts

$$k_{E,n}^{-1} = k_E^{-1} \left(f_2 Z^n + \frac{f_3}{1 - n + n\phi_3^T} \right) \quad (38)$$

SCHEME VII. Conformational Equilibrium Model for Proton Inventories of k_E of AChE Catalysis


for the possibility that a solvent isotope effect accompanies the AChE isomerization step k_2 due to solvation changes. A Z -term isotope effect for k_2 could account for the difference in the intrinsic isotope effects for ONCA hydrolysis that resulted from fitting the proton inventory to eq 25 ($D_2O k_3 = 2.3$) and from the DMSO inhibition experiment ($D_2O k_3 = 1.95$). If the intrinsic isotope effect is 1.95, one can generate a fit that is indistinguishable from that in Figure 2 by using eq 38 with $f_2 = f_3 = 0.5$ and $Z = 0.9$. Other combinations of f_3 and Z produce fits that cannot accommodate both the observed isotope effect and the curvature of the proton inventory. Therefore, if there is a Z -term isotope effect for k_2 , it is not very great, and the indication is that k_2 and k_3 both contribute prominently to rate determination. The virtual transition-state model remains intact.

A fourth model that can accommodate the upward-bowing proton inventory of Figure 2 is one in which there are two conformations of the enzyme that have different activities. This situation is outlined in Scheme VII, which is a more general form of the conformational equilibrium model of Scheme V that was proposed by Rosenberry and Bernhard.¹⁰⁹ Note that the mechanism in Scheme VII assumes that equilibration of E^0 and E^* and of ES^0 and ES^* is rapid. If this is not so, one has the mechanism of Scheme II from which the virtual transition-state model comes. Equations 39–43 of Scheme VII outline the derivation of the dependence of $k_{E,n}$ on n (eq 43). As eq 42 shows, k_E is a weighted average of the conformation-dependent k_E^0 and k_E^* . The weighting factors are those of eq 41, which account for the contributions of E^0 and E^* to the conformational equilibrium. In eq 43, k_E^* must be $> k_E^0$ for $\phi^T < 1$ or $D_2O k_E > 1$ will not result. The simplest situation, one in which the solvent isotope effect on K_0 arises from a protonic site in E^* with a fractionation factor ϕ^* , is assumed. If instead k_E^0 and/or k_E^* are subject to solvent isotope effects that arise from one or more transition-state protons (cf. eq 19), a linear or downward-bowing proton inventory for k_E will result. Computer simulations of eq 43 generate fits of the ONCA proton inventory that are indistinguishable from that of Figure 2. For simulations in which k_E^*/k_E^0 covers a range from 3 to 1000, $K_0 = 1$ –2 and $\phi^* = 0.26$ –0.45.¹³³ Therefore, in order for the conformational equilibrium model to operate, the fractionation factor for E^* must

take on values that are unprecedented for the prototropic functionalities of amino acid side chains (save RSH^{119–123}). In fact, fractionation factors in the range 0.26–0.45 are common for transition-state proton transfers between the heteroatoms O, N, and S.^{119–121} However, Kreevoy et al.¹³² described fractionation factors in this range for short, strong H bonds in assemblies of the type $[A-H-A]^-$ in organic solvents, where A is such as F^- or p -nitrophenoxide. An additional weakness of the conformational equilibrium model is its inability to explain the variability of pK_a values for k_E of AChE-catalyzed hydrolysis of neutral esters^{2,20,27} and anilides.^{18,20}

The salient feature of the foregoing discussion of nonlinear and upward-bulging proton inventories is that none of the alternate models is capable of accounting for the diverse observations for k_E of AChE reactions. Only the virtual transition-state model readily explains the nonlinear proton inventories, the dependence of $D_2O k_E$ and $D k_E$ on substrate reactivity, the pH- k_E behavior, the dependence of $D_2O k_E$ on DMSO inhibition, and the nonlinear Eyring plots. This versatility makes the virtual transition-state model easily the one of choice.

3. Solvent Isotope Effects and Effective (Virtual) Reactant State for k_{ES}

As the data in Table V indicate, $D_2O k_{ES}$ values are invariably larger than the corresponding $D_2O k_E$ values. This is especially significant for the anilides, because their k_{ES} values are smaller than those of acyl-similar esters (compare ONFA and PMPF, ONA and ONPA, ONCA and PCA), and therefore k_{ES} for anilides must be rate limited by a transition state in the acylation stage of catalysis.^{21,134} That $D_2O k_{ES} > D_2O k_E$ necessitates that the solvent isotope-sensitive step comes after the solvent isotope-insensitive step. This order of microscopic events was assumed when the mechanism of Schemes II and VI was formulated. Furthermore, the greater expression of the intrinsic isotope effect $D_2O k_3$ in $D_2O k_{ES}$ than in $D_2O k_E$ allows one to calculate the distribution of stable states ES_1 and ES_2 for ONCA and ONFA. For rate-determining acylation eq 16 reduces to eq 44 at $pH \gg pK_a$. From this equation one can

$$k_{ES} = \frac{k_2 k_3}{k_{-2} + k_2 + k_3} \quad (44)$$

derive eq 45 for the solvent isotope effect for k_{ES} . The

$$D_2O k_{ES} = \frac{D_2O k_3 + R}{1 + R}, \text{ where } R = \frac{C}{1 + k_2/k_{-2}} \quad (45)$$

factor $1 + k_2/k_{-2}$ accounts for the distribution of bound states between ES_1 and ES_2 . Thus, from eqs 28 and 45, eq 46 follows. Since the requisite isotope effects and

$$\frac{D_2O k_{ES} - 1}{D_2O k_E - 1} = \frac{1 + C}{1 + R} \quad (46)$$

C values are available for ONCA and ONFA, R can be calculated from eq 46 and k_2/k_{-2} can be calculated from eq 45. These results and other data are contained in Table VII. The values of k_2/k_{-2} show that at substrate saturation AChE is predominantly in the ES_2 state. Therefore, the k_3 transition state is more rate determining for k_{ES} than for k_E , as the greater expression of

TABLE VII. Reaction Dynamics and Thermodynamics for AChE-Catalyzed Anilide Hydrolyses^a

parameter	substrate		
	ONCA	ONA	ONFA
C^b	2.0 (± 0.2)	1.4 (± 0.2)	
R	2.0 (± 0.4)	1.4 (± 0.2)	2.0 (± 0.4)
k_2/k_{-2}	0.25 (± 0.10)		0.5 (± 0.3)
ΔG_E^* , kcal mol ⁻¹	7.0 (± 3.5)		3.0 (± 2.7)
ΔG_2^* , kcal mol ⁻¹	18.8	20.3	21.2
ΔG_3^* , kcal mol ⁻¹	18.6	20.0	21.0
$\Delta G_{ES_1}^*$, kcal mol ⁻¹	18.1	19.8	20.5
$\Delta G_{ES_2}^*$, kcal mol ⁻¹	4.0	5.9	4.5
ΔG_1 , kcal mol ⁻¹	4.7		4.9
ΔG_2 , kcal mol ⁻¹	4.2		4.9

^aFree energy changes were calculated as described in the text and as detailed in ref 21. ^bThe first row of commitments was calculated by using eq 28 and $D_2O k_E$ values from Table V. Intrinsic isotope effects for k_3 used in the calculations are those for the DMSO-inhibited ONCA and ONA reactions; see ref 21 for elaboration. The second row of commitments are from Table VI.

$D_2O k_3$ in $D_2O k_{ES}$ necessitates. It is important to note, however, that the phenomenological transition state for k_{ES} is still a virtual transition state. The weighting factors in this case are given by eq 47. The weighting

$$f_2 = \frac{R}{R+1} \quad f_3 = \frac{1}{R+1} \quad (47)$$

factors are determined not only by the relative free energies of the k_2 and k_3 transition states, as reflected in C , but also by the relative free energies of ES_1 and ES_2 , as reflected in k_2/k_{-2} .

4. Free Energy Diagram for Anilide Hydrolyses

The values of C and k_2/k_{-2} that were determined from solvent isotope effects and proton inventories can be used to construct the free energy diagram for anilide hydrolysis. To calculate the free energies of the k_2 and k_3 transition states, one first calculates the phenomenological free energy of activation¹²⁵ as shown in eq 48.

$$\Delta G_E^* = -RT \ln (k_E h / k_B T) \quad (48)$$

In this equation k_B and h are Boltzmann's and Planck's constants, respectively. ΔG_E^* values for anilides are presented in Table VII. All ΔG calculations in the table refer to a substrate standard state of 1 μ M and equal standard states (e.g., 1 nM) for E and ES complexes, including transition states. The free energy equivalent of eq 6 of Chart VI for a virtual transition state is

$$e^{\Delta G_E^*/RT} = e^{\Delta G_2^*/RT} + e^{\Delta G_3^*/RT} \quad (49)$$

Since $C = k_3/k_{-2}$ and the k_2 transition state is the k_{-2} transition state, the relative free energies of the k_2 and k_3 transition states are

$$RT \ln C = \Delta G_2^* - \Delta G_3^* \quad (50)$$

Equations 49 and 50 are used to solve for the individual free energies of activation in terms of measurable quantities.

$$\Delta G_2^* = \Delta G_E^* + RT \ln f_2 \quad (51)$$

$$\Delta G_3^* = \Delta G_E^* + RT \ln f_3 \quad (52)$$

The relationship among f_2 , f_3 , and C is given in eq 29.

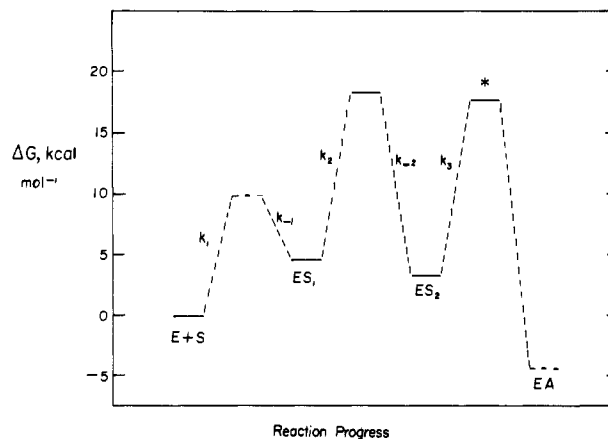


Figure 7. Free energy diagram for AChE-catalyzed hydrolysis of ONCA. Reproduced with permission from ref 21. Copyright 1987 American Chemical Society.

The phenomenological free energy change for stable state formation is calculated as follows.

$$\Delta G_{ES} = RT \ln K_m \quad (53)$$

K_m^{-1} comes from dividing eq 3 by eq 44

$$K_m^{-1} = K_1^{-1} + [K_2(1 + C)]^{-1} = K_1^{-1} \left(1 + \frac{k_2/k_{-2}}{1 + C} \right) \quad (54)$$

In this equation $K_1 = k_{-1}/k_1$ and $K_2 = k_{-1}k_{-2}/k_1k_2$ are the dissociation constants of ES_1 and ES_2 , respectively. Equation 54 shows that K_m is comprised of K_1 and $K_2(1 + C)$, the respective Michaelis constants for ES_1 and ES_2 . Therefore, the microscopic free energy changes for ES_1 and ES_2 formations are

$$\Delta G_1 = RT \ln K_1 \quad \Delta G_2 = RT \ln [K_2(1 + C)] \quad (55)$$

Eqs 53–55 are used to derive eq 56 and 57 for the stable state ΔG values in terms of measurable quantities.

$$\Delta G_1 = \Delta G_{ES} + RT \ln \left(1 + \frac{k_2/k_{-2}}{1 + C} \right) \quad (56)$$

$$\Delta G_2 = \Delta G_1 + RT \ln [(k_{-2}/k_2)(1 + C)] \quad (57)$$

Table VII contains ΔG values that were calculated from eqs 51, 52, 56, and 57. The ΔG values for AChE-catalyzed hydrolysis of ONCA were used to construct the free energy diagram of Figure 7. As the free energy diagram shows, stable states of similar free energies precede transition states of similar free energies. Hence, the acylation stage of AChE catalyzed anilide hydrolyses displays matched internal thermodynamics.^{32,135}

D. Virtual Transition States for Ester Hydrolyses

1. Probes of Virtual Transition States for k_E

Unlike anilides, none of the solvent isotope effect measurements done in my laboratory for k_E of ester substrates indicates significant rate determination by the chemical k_3 transition state, as data in Table V for ONPA through PMPCA demonstrate.^{19,20} Moreover, for ONPA¹⁹ and PMPF²⁰ the respective β -D and α -D secondary isotope effects are within experimental error of unity, which indicates that there is little nucleophilic interaction between AChE and the carbonyl carbon of the substrate in the transition state for k_E . These iso-

tope effects, therefore, support a model in which k_1 and/or k_2 , which respectively monitor substrate binding and $ES_1 \rightarrow ES_2$ isomerization, are predominantly rate determining. In this case, the commitment to catalysis C is given by eq 3, and measures the tendency of ES_2 to proceed to EA via the chemical k_3 transition state vs. reversion to $E + S$ via the kinetically significant k_1 and/or k_2 transition states. Though the lack of a solvent isotope effect for k_E precludes determination of C , a reasonable estimate can be made. Consider the case of PMPF, for which $D_2O k_E = 1.09 \pm 0.01$. If the intrinsic effect is $D_2O k_3 \sim 2$, which is typical for anilides and PNPA (cf. Table VI) and is the average $D_2O k_{ES}$ for esters (cf. Table V), then according to eq 28 $C \sim 10$ is required to produce $D_2O k_E = 1.09$. This estimate of C indicates that k_3 is $<10\%$ rate determining, which is supported by $D k_E = 0.99 \pm 0.01$.

That k_E for esters is rate limited by a virtual transition state is supported by additional observations: (1) the Eyring plot for k_E of AChE-catalyzed hydrolysis of PMPF is upward-bowing,²⁰ as discussed earlier for anilides. (2) $D_2O k_E$ for PMPF increases from 1.02 ± 0.03 at 35 °C to 1.20 ± 0.08 at 15 °C. This temperature sensitivity of the isotope effect is consistent with partial exposure of the k_3 transition state at lower temperature. (3) The pH dependence of k_E for neutral esters generally gives pK_a values in the range 5.2–5.8,^{2,20,27,76,77} which is consistent with suppression of the intrinsic $pK_a = 6.3$ of the active site histidine by significant rate determination by the pH-insensitive k_1 and/or k_2 steps. As was done for anilides, an estimate of the intrinsic pK_a for k_E of PMPF hydrolysis can be calculated by using eq 30 and the C value estimated in the preceding paragraph. The result is an intrinsic $pK_a \sim 6.6$ (cf. Table VI). (4) For PNPA, the least reactive aryl ester in Table V, Rosenberry²⁷ measured $D_2O k_E = 1.93$ and Hogg et al.⁴³ measured $D_2O k_E = 1.56$. Both determinations indicate that there is significant exposure of the chemical k_3 transition state to rate determination. The proton inventory for PNPA⁴³ is well described by nonlinear-least-squares fitting to eq 25, as discussed earlier. The corresponding virtual transition-state parameters are contained in Table VI. Also, Rosenberry²⁷ measured $D_2O k_E \sim 2$ for AChE-catalyzed hydrolysis of methyl acetate, the least reactive substrate in Table V; this isotope effect is consistent with considerable rate determination by the k_3 transition state.

2. Probes of Virtual Transition States for k_{ES}

Unlike k_E , k_{ES} for ester substrates is prominently rate limited by chemical transition states. This is suggested by the sizeable $D_2O k_{ES}$ values of Table V for ONPA through PMPFA, and by inverse β -D and α -D secondary isotope effects for k_{ES} of ONPA and PMPF, respectively.^{19,136} The secondary isotope effects are consistent with nucleophilic AChE interaction at the carbonyl carbon in the transition state for k_{ES} .^{126–130} Moreover, the k_{ES} values for acyl-similar esters (ONPA and PA, PCA and PMPFA) are similar, which suggests that k_{ES} is prominently rate limited by deacylation (k_4 in Schemes II and VI). Therefore, for ester substrates, eq 15 simplifies to eq 58 at $pH \gg pK_a$. If eq 58 is

$$k_{ES} = \frac{k_3 k_4}{k_3 + k_4} \quad (58)$$

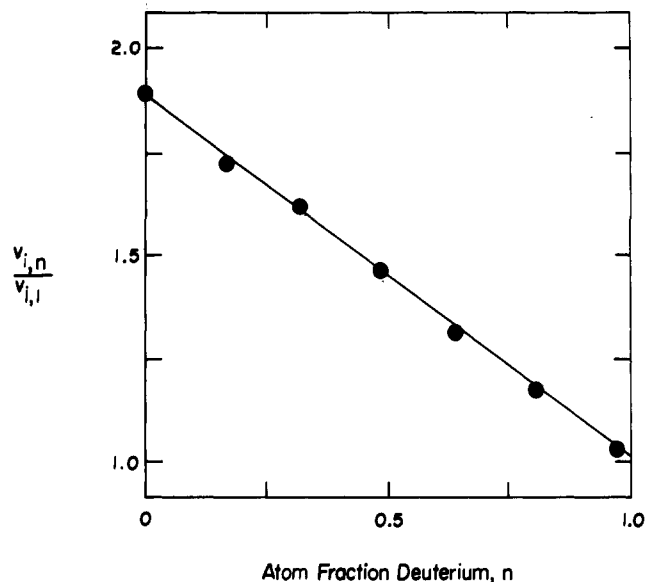


Figure 8. Proton inventory for AChE-catalyzed hydrolysis of ONPA, plotted as partial solvent isotope effects on V_i . V_i 's were determined at $[ONPA] \gg K_m$. See ref 19 for details.

correct, k_{ES} is rate limited by a virtual transition state that is comprised of the transition states of the k_3 and k_4 steps. The discussion that follows supports this assignment for k_{ES} .

The proton inventories for k_{ES} of AChE-catalyzed hydrolysis of ONPA (Figure 8) and PCA are linear,¹⁹ which indicates that AChE acts as a one-proton catalyst in the respective transition states. Kovach et al.²² reached a similar conclusion on the basis of linear proton inventories for AChE-catalyzed hydrolysis of PA. These results are consistent with the description of proton inventories for k_{ES} of ester substrates by eq 59, a particular case of eq 19. However, the situation is

$$k_{ES,n} = k_{ES}(1 - n + n\phi^T) \quad (59)$$

not as simple as first meets the eye. Froede and Wilson²⁶ recently showed that k_{ES} of AChE-catalyzed hydrolysis of ACh is 68% rate limited by deacylation, k_4 . As Acheson et al.¹⁹ showed, one can calculate the fraction of rate determination by k_4 for alternate acetate ester substrates from the ratio of k_{ES} for the alternate substrate to that for ACh. Therefore, since k_{ES} for PA is 10% higher than that for ACh,^{2,27} k_{ES} for PA is 75% rate limited by deacylation.²² In turn, the ONPA reaction is 56% rate limited by deacylation because k_{ES} for ONPA is 74% of that for PA. One is then obliged to describe the transition state for k_{ES} of ONPA hydrolysis as a virtual transition state that is comprised of nearly equal contributions from acylation and deacylation,¹⁹ and the correct expression for describing the ONPA proton inventory of Figure 8 is that of eq 60.

$$k_{ES,n}^{-1} = k_{ES}^{-1} \left(\frac{0.44}{1 - n + n\phi_3^T} + \frac{0.56}{1 - n + n\phi_4^T} \right) \quad (60)$$

The fractionation factors ϕ_3^T and ϕ_4^T are those of the general acid–base proton bridges that stabilize the acylation and deacylation transition states, respectively. The linear ONPA proton inventory suggests that the solvent isotope effects $D_2O k_3 = 1/\phi_3^T$ and $D_2O k_4 = 1/\phi_4^T$ are nearly the same, so that eq 60 reduces to eq 59. The

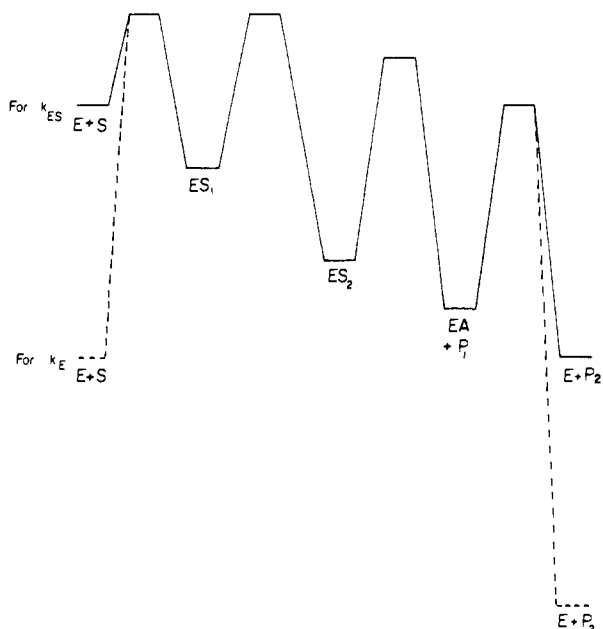


Figure 9. Qualitative free energy diagram for AChE-catalyzed hydrolysis of ONPA.

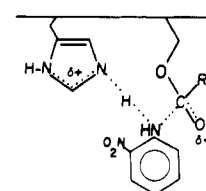
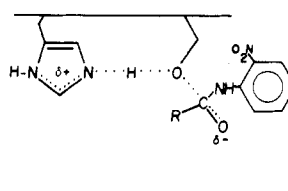
Eyring plot for k_{ES} of AChE-catalyzed hydrolysis of ONPA is nonlinear and upward-bowing,¹⁹ which is also indicative of a virtual transition state comprised of serial microscopic transition states. However, $D_2O k_{ES}$ does not vary with temperature, which supports the contention that $D_2O k_3 \sim D_2O k_4$. It appears then that the solvent isotope-insensitive k_2 transition state does not make an important contribution to rate determination of the acylation component of k_{ES} . The pH- k_{ES} profile for ONPA depends on a $pK_a = 6.31 \pm 0.03$,¹⁹ which agrees with the intrinsic pK_a of the active site histidine^{2,25,27} and again suggests that the pH-insensitive k_2 step does not make an important contribution to rate limitation of the acylation component of k_{ES} .

3. Free Energy Diagram for Ester Hydrolyses

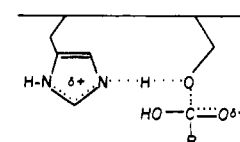
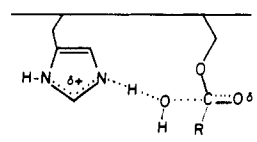
A qualitative free energy diagram for aryl ester hydrolyses is shown in Figure 9. Some quantitative features of the diagram for ONPA hydrolysis can be gleaned from experimental data. The free energies of activation of the chemical k_3 and k_4 steps are nearly the same, since each step contributes about equally to rate determination of k_{ES} . The stable states ES_2 and EA ramp downhill in free energy even in the presence of *o*-nitrophenol because product inhibition is not observed.¹⁹ Moreover, the k_3 transition state is ~ 1.4 kcal/mol lower in free energy than is the k_2 and/or k_1 transition state, because the commitment C (cf. eq 6) must be ~ 10 so that $D_2O k_3 \sim 2$ is not expressed in $D_2O k_{ES}$. Since the virtual transition state for k_{ES} is not prominently rate limited by k_2 , k_2/k_{-2} must be large and $k_2 \gg k_3$. These conditions prevent the ES_1 complex from accumulating at substrate saturation. The free energy diagram thus accounts for the isotope effects for reactions of ONPA and other esters. When k_E is measured, the reactant state is $E + S$, and there are no substrate or solvent isotope effects because k_1 and/or k_2 is rate determining. When k_{ES} is measured, the reactant state is $ES_2 + EA$, and the isotopically sensitive k_3 and k_4 transition states are rate limiting. The free energy diagram for esters shares the interesting feature of

CHART VIII. Chemical Transition States for AChE Catalysis

Acylation



Deacylation



matched internal thermodynamics^{32,135} with the free energy diagram of Figure 7, albeit with the transition-state and stable-state free energies ramping downhill as described by Benner and co-workers¹³⁷ for essentially irreversible reactions.

E. Structural Features of Chemical Transition States

All AChE proton inventories conducted to date that directly probe intrinsic structural features of chemical transition states are linear. These include proton inventories of k_E for DMSO-inhibited AChE-catalyzed hydrolysis of ONA and ONCA²¹ and proton inventories of k_{ES} for ONPA, PCA,¹⁹ and PA²² hydrolyses. Hence, AChE stabilizes chemical transition states via simple general acid-base catalysis, with the likely involvement of proton bridges between the imidazole side chain of the active site histidine and the substrate-derived portion of the transition state. Since AChE catalyzes acyl transfer reactions, which generally proceed via tetrahedral intermediates (cf. Scheme III),¹³⁸ there are at least four chemical transition states, two each in the acylation and deacylation stages of catalysis.¹³⁹ Chart VIII shows structures of chemical transition states that are consistent with the substrate and solvent isotope effects presented in this review.

There are two features of the chemical transition states of Chart VIII that deserve comment. The first feature comes from substrate secondary isotope effects, which are consistent with partial $sp^2 \rightarrow sp^3$ rehybridization in both the acylation and deacylation transition states.¹²⁶⁻¹³⁰ The $D k_{ES}$ values for ONPA and PMPF indicate that fractional rehybridization is 0.3 ± 0.1 .^{19,136,140} However, since both acylation and deacylation contribute to rate determination of k_{ES} for ONPA, there are two extreme possibilities for the indicated degree of rehybridization. One is that fractional rehybridization of 0.3 is an intrinsic structural feature of both the acylation and deacylation transition states. The second is that in the acylation (or deacylation) transition state the carbonyl carbon has undergone a fractional rehybridization of 0.6, while there is no rehybridization in the deacylation (or acylation) transition state. Since acylation and deacylation are comparably rate determining for k_{ES} of ONPA, this latter possibility

corresponds to an apparent fractional rehybridization of 0.3 for the virtual transition state (cf. eq 13). Which of these two possibilities operates cannot be decided at present. The α -D secondary isotope effect $^Dk_{ES} = 0.85 \pm 0.06$ for ONFA, which is consistent with an acylation transition state that involves a fractional $sp^2 \rightarrow sp^3$ rehybridization of 0.5 ± 0.2 . However, the intrinsic α -D effect should be more inverse and the fractional rehybridization more complete, since the observed effect monitors a virtual transition state. The α -D effect $^Dk_E = 0.88 \pm 0.02$ for ONFA also indicates that significant substrate rehybridization has occurred in the acylation transition state. The estimated intrinsic effect was $^Dk_3 = 0.64 \pm 0.10$, which is consistent with complete $sp^2 \rightarrow sp^3$ rehybridization in the chemical k_3 transition state. Therefore, AChE catalysis involves quasi-tetrahedral chemical transition states, which one expects for an addition-elimination mechanism.

The second feature of the chemical transition states for AChE catalysis is the nature of the enzyme's general acid-base catalytic machinery. Unlike the serine proteases, which behave as two-proton "charge-relay"⁶⁴ catalysts for reactions of peptide substrates,^{17,79-82} AChE always behaves as a one-proton catalyst. This prototropic catalysis includes the physiological deacetylation reaction, as the linear proton inventories for ONPA¹⁹ and PA²² demonstrate. The serine protease analogy thus does not apply to the AChE acid-base catalytic machinery, which suggests that the AChE active site does not contain an Asp-His-Ser triad that characterizes the serine protease active site.^{7-9,64} This is not surprising since serine proteases and AChE have little sequence homology,^{61,66} and AChE does not have Asp, His, and Ser residues comparably positioned in the primary sequence.^{61,65,66} Therefore, AChE structure and reaction dynamics support each other in nixing the serine protease analogy.

IV. AChE Reaction Dynamics and the Evolution of Enzyme Catalytic Power

As mentioned earlier, k_E for AChE-catalyzed hydrolysis of the physiological substrate ACh is diffusion controlled, which is a hallmark of reaction dynamics for enzymes whose catalytic power cannot be greatly enhanced by further evolution. Albery and Knowles^{32,135} described a scenario for the evolution of enzyme catalytic power in which the free energies of successive transition states are eventually nearly matched and comparable to the unrodible diffusional barrier for substrate binding, and in which the free energies of bound states are comparable. Enzyme reactions that have such free energetics are said to display "matched internal thermodynamics". One might expect that AChE-catalyzed hydrolysis of ACh would display this kind of reaction thermodynamics. The surprise comes when one considers the free energy diagrams for hydrolyses of anilides (Figure 7) and aryl esters (Figure 9). The diagram for anilides shows that internal transition-state free energies are matched, as are stable-state free energies. Admittedly, the free energies of the k_2 and k_3 transition states are somewhat higher than that of the k_1 transition state (i.e., binding does not contribute significantly to rate determination for k_E), but one might imagine that the anilide free energy diagram is reminiscent of an earlier stage in the evolution of

AChE catalytic power. Matched internal thermodynamics appear to mark the reactions of all three anilides studied thus far, even though k_E for ONFA, the least reactive, is $>10^5$ -fold less than that of ACh.²⁰ The free energy diagram for aryl esters extends these speculations to the deacylation stage of catalysis. For ONPA, the microscopic free energy barriers for the chemical steps of acylation and deacylation are matched, and the free energies of the k_3 transition state on the one hand and the k_1 and/or k_2 transition state on the other are within 1-2 kcal/mol. ACh shares some of these features, in that k_3 and k_4 are comparable.²⁶

It is, therefore, interesting to speculate that in the dim past AChE was an evolving broad-spectrum hydrolytic enzyme. This supposition is supported by the extensive homology in the active site regions of *T. californica* AChE and equine aliesterase,⁶⁶ whose physiological function is unrelated to that of AChE. This supposition is in accord with AChE's promiscuous substrate specificity, which requires a conformationally plastic enzyme active site. As discussed in this review, structural studies of the enzyme support such conformational plasticity (cf. II. AChE Structure C. Active Site Structure). Moreover, reaction dynamics for k_E of various substrates are consistent with an induced-fit step that precedes chemical catalysis and that adjusts the active site to stabilize the k_3 transition state.^{2,18-21,27} AChE may have come with catalytic power nearly optimal upon its physiological substrate relatively recently in evolution and in response to the need for neurotransmission in the primeval nervous system. That is, perhaps AChE catalytic power converged on a substrate (ACh) whose physiological role was also evolving.

V. Future Directions

The ability to characterize the chemistry and reaction dynamics of AChE catalysis is in its infancy. The next several years should witness a significant increase in our understanding of the structural basis of AChE catalysis and catalytic power. In particular, the methods described in this review will be extended to ACh and its close structural homologues so that eventually the reaction dynamics, thermodynamics, and intrinsic chemical transition-state structures of physiological AChE catalysis are defined. The complete amino acid sequence of an AChE has only recently been determined.⁶¹ One can imagine that cloning of the AChE gene and determination of the X-ray structure of the enzyme are not far behind. Knowledge of the enzyme's amino acid sequence will aid greatly in interpreting the effects of chemical modifications of specific amino acids on AChE catalysis and ligand interactions. Site-directed mutagenesis of AChE should eventually prove a powerful tool for delineating the structural basis of the complex reaction dynamics, enzyme conformational dynamics and ligand interactions discussed herein. For example, the importance of an active site anionic locus can be probed by this technique. The ability to construct free energy diagrams from isotope effects and other kinetics should prove especially powerful in interpreting the effects of chemical and mutagenic amino acid modifications. It seems highly likely that by using recently developed techniques for probing AChE structure-function, coupled with techniques that should come online within the next few years, an understand-

ing of enzyme catalytic power that is virtually unparalleled in hydrolytic enzymology will emerge.

Acknowledgments. The lion's share of investigations in my laboratory that are described in this review was performed by the following individuals: Dr. Scott Acheson, Dr. Paul Barlow, Dimitra Dedopoulou, Gerry Lee, and Mike Swanson. Their hard work is gratefully acknowledged. The following investigators and their co-workers kindly provided reprints and preprints that greatly helped in preparation of this review: Dr. Ildiko Kovach, Professors Terrone Rosenberry (thanks to Bill Roberts), Harvey Berman, Irwin B. Wilson, Urs Brodbeck, and Richard L. Schowen. I acknowledge the support of the National Institutes of Health for investigations of AChE catalysis (Grant NS21334) and for a Research Career Development Award (Grant HL01583) that provides sufficient relief from other demands so that a review such as this could be completed in a timely fashion.

Registry No. AChE, 9000-81-1.

VI. References and Notes

- Abbreviations used: AChE, acetylcholinesterase; ACh, acetylcholine; ATCh, acetylthiocholine; DMBA, 3,3-dimethylbutyl acetate; 2-PAM, 2-pyridinealdoxime methiodide; k_E , k_{cat}/K_m ; k_{ES} , k_{cat} ; K_i , enzyme-inhibitor dissociation constant; K_d , enzyme-ligand dissociation constant; PA, phenyl acetate; ONPA, *o*-nitrophenyl acetate; PCA, phenyl chloroacetate; PMPCA, *p*-methoxyphenyl chloroacetate; ONA, *o*-nitroacetanilide; ONCA, *o*-nitrochloroacetanilide; PMPF, *p*-methoxyphenyl formate; PNPA, *p*-nitrophenyl acetate; ONFA, *o*-nitroformanilide; $D_2^0k_E$, $D_2^0k_{ES}$, solvent deuterium kinetic isotope effects for k_E and k_{ES} , respectively; D^Rk_{ES} , D^Rk_E , substrate secondary deuterium kinetic isotope effect for k_{ES} and k_E , respectively; α -D, β -D, α - and β -deuterium, respectively.
- Rosenberry, T. L. *Adv. Enzymol. Relat. Areas Mol. Biol.* **1975**, *43*, 103-218.
- Taylor, P. In *Pharmacological Basis of Therapeutics*; Gilman, A. G., Goodman, L. S., Murad, F., Eds.; MacMillan: New York, 1985; pp 110-129.
- Summers, W. K.; Majovski, L. V.; Marsh, G. M.; Tachiki, K.; Kling, A. N. *Engl. J. Med.* **1986**, *315*, 1241-1245.
- Thai, L. J.; Fuld, P. A.; Masur, D. M.; Sharpless, N. S. *Ann. Neurol.* **1983**, *13*, 491-496.
- Marchbanks, R. M. *J. Neurochem.* **1982**, *39*, 9-15.
- Stroud, R. M. *Sci. Am.* **1974**, *231*, 74-88.
- Blow, D. M. *Acc. Chem. Res.* **1976**, *9*, 145-152.
- Kraut, J. *Ann. Rev. Biochem.* **1977**, *46*, 331-358.
- Schowen, R. L. In *Transition States of Biochemical Processes*; Gandour, R. D., Schowen, R. L., Eds.; Plenum: New York, 1978; pp 77-114.
- Stein, R. L. *J. Org. Chem.* **1981**, *46*, 3328-3330.
- Stein, R. L.; Fujihara, H.; Quinn, D. M.; Fischer, G.; Küllertz, G.; Barth, A.; Schowen, R. L. *J. Am. Chem. Soc.* **1984**, *106*, 1457-1461.
- Quinn, D. M.; Elrod, J. P.; Ardis, R.; Friesen, P.; Schowen, R. L. *J. Am. Chem. Soc.* **1980**, *102*, 5358-5365.
- Stein, R. L. *J. Am. Chem. Soc.* **1985**, *107*, 5767-5775.
- Stein, R. L. *J. Am. Chem. Soc.* **1985**, *107*, 6039-6042.
- Stein, R. L. *J. Am. Chem. Soc.* **1985**, *107*, 7768-7769.
- Stein, R. L.; Strimpler, A. M.; Hori, H.; Powers, J. C. *Biochemistry* **1987**, *26*, 1305-1314.
- Quinn, D. M.; Swanson, M. L. *J. Am. Chem. Soc.* **1984**, *106*, 1883-1884.
- Acheson, S. A.; Dedopoulou, D.; Quinn, D. M. *J. Am. Chem. Soc.* **1987**, *109*, 239-245.
- Acheson, S. A.; Barlow, P. N.; Lee, G. C.; Swanson, M. L.; Quinn, D. M. *J. Am. Chem. Soc.* **1987**, *109*, 246-252.
- Barlow, P. N.; Acheson, S. A.; Swanson, M. L.; Quinn, D. M. *J. Am. Chem. Soc.* **1987**, *109*, 253-257.
- Kovach, I. M.; Larson, M.; Schowen, R. L. *J. Am. Chem. Soc.* **1986**, *108*, 3054-3056.
- Northrop, D. B. *Biochemistry* **1975**, *14*, 2644-2651.
- Northrop, D. B. In *Isotope Effects on Enzyme-Catalyzed Reactions*; Cleland, W. W., O'Leary, M. H., Northrop, D. B., Eds.; University Park: Baltimore, 1977; pp 122-152.
- Froede, H. C.; Wilson, I. B. In *The Enzymes*, 3rd ed.; Boyer, P. D., Ed.; Academic: New York, 1971; Vol. 5, pp 87-114.
- Froede, H. C.; Wilson, I. B. *J. Biol. Chem.* **1984**, *259*, 11010-11013.
- Rosenberry, T. L. *Proc. Natl. Acad. Sci. U.S.A.* **1975**, *72*, 3834-3838.
- In this review "acylation" has two meanings, which depend on the context. The rate constant k_E always refers to conversion of E + S to the rate-determining transition state that precedes or is coincident with the first irreversible event in the mechanism, which for AChE is no later than the release of P₁ that completes the acylation stage of catalysis. When k_{ES} is measured, acylation refers to those components of the rate constant that arise from kinetically significant transition states that lie between the initial Michaelis complex ES₁ and the acylenzyme EA.
- Fisher, L. M.; Albery, W. J.; Knowles, J. R. *Biochemistry* **1986**, *25*, 2529-2537.
- Rosenberry, T. L.; Bernhard, S. A. *Biochemistry* **1971**, *10*, 4114-4120.
- Bazelyansky, M.; Robey, E.; Kirsch, J. F. *Biochemistry* **1986**, *25*, 125-130.
- Knowles, J. R.; Albery, W. J. *Acc. Chem. Res.* **1977**, *10*, 105-111.
- Nolte, H. J.; Rosenberry, T. L.; Neumann, E. *Biochemistry* **1980**, *19*, 3705-3711.
- Rosenberry, T. L.; Neumann, E. *Biochemistry* **1977**, *16*, 3870-3878.
- Naveh, M.; Bernstein, Z.; Segal, D.; Shalitin, Y. *FEBS Lett.* **1981**, *134*, 53-56.
- Bender, M. L.; Stoops, J. K. *J. Am. Chem. Soc.* **1965**, *87*, 1622-1623.
- Ellman, G. L.; Courtney, K. D.; Andres, V., Jr.; Featherstone, R. M. *Biochem. Pharmacol.* **1961**, *7*, 88-95.
- Hillman, G. R.; Mautner, H. G. *Biochemistry* **1970**, *9*, 2633-2638.
- Moore, D. E.; Hess, G. P. *Biochemistry* **1975**, *14*, 2386-2389.
- Massoulié, J.; Rieger, F. *Eur. J. Biochem.* **1969**, *11*, 441-455.
- Wilson, I. B.; Cabib, E. *J. Am. Chem. Soc.* **1956**, *78*, 202-207.
- The OH⁻-catalyzed hydrolysis of *p*-nitroacetanilide has an observed rate constant of $4.18 \times 10^{-6} \text{ s}^{-1}$ when $[\text{OH}^-] = 0.01 \text{ N}$. For the structurally analogous ester *p*-nitrophenyl acetate the observed rate constant, calculated from data in ref 43, is 0.085 s^{-1} under the same conditions. Therefore, the reactivity for the ester is 2×10^4 fold greater than for the anilide.
- Hogg, J. L.; Elrod, J. P.; Schowen, R. L. *J. Am. Chem. Soc.* **1980**, *102*, 2082-2086.
- Hasan, F. B.; Cohen, S. G.; Cohen, J. B. *J. Biol. Chem.* **1980**, *255*, 3898-3904.
- Kramer, D. N.; Gamson, R. M. *Anal. Chem.* **1958**, *30*, 251-254.
- Rosenberry, T. L. In *The Enzymes of Biological Membranes*; Martonosi, A. N., Ed.; Plenum: New York, 1985; Vol. 3, pp 403-429.
- Massoulié, J.; Bon, S. *Annu. Rev. Neurosci.* **1982**, *5*, 57-106.
- Rosenberry, T. L.; Barnett, P.; Mays, C. *Neurochem. Int.* **1980**, *2*, 135-147.
- Gordon, M. A.; Carpenter, D. E.; Wilson, I. B. *Mol. Pharmacol.* **1978**, *14*, 266-270.
- Ott, P.; Lustig, A.; Brodbeck, U.; Rosenbusch, J. P. *FEBS Lett.* **1982**, *138*, 187-189.
- Brimijoin, S.; Mintz, K. P. *Biochim. Biophys. Acta* **1985**, *828*, 290-297.
- Fambrough, D. M.; Engel, A. G.; Rosenberry, T. L. *Proc. Natl. Acad. Sci. U.S.A.* **1982**, *79*, 1078-1082.
- Brimijoin, S.; Mintz, K. P.; Alley, M. C. *Mol. Pharmacol.* **1983**, *24*, 513-520.
- Dutta-Choudhury, T. A.; Rosenberry, T. L. *J. Biol. Chem.* **1984**, *259*, 5653-5660.
- Kim, B. H.; Rosenberry, T. L. *Biochemistry* **1985**, *24*, 3586-3592.
- Haas, R.; Brandt, P. T.; Knight, J.; Rosenberry, T. L. *Biochemistry* **1986**, *25*, 3098-3105.
- Roberts, W. L.; Rosenberry, T. L. *Biochem. Biophys. Res. Commun.* **1985**, *133*, 621-627.
- Rosenberry, T. L.; Roberts, W. L.; Haas, R. *Fed. Proc. Fed. Am. Soc. Exp. Biol.* **1986**, *45*, 2970-2975.
- Futerman, A. H.; Fiorini, R. M.; Roth, E.; Low, M. G.; Silman, I. *Biochem. J.* **1985**, *226*, 369-377.
- Majumdar, R.; Balasubramanian, A. S. *Biochem. Pharmacol.* **1985**, *34*, 4109-4115.
- Schumacher, M.; Camp, S.; Maulet, Y.; Newton, M.; MacPhee-Quigley, K.; Taylor, S. S.; Friedmann, T.; Taylor, P. *Nature (London)* **1986**, *319*, 407-409.
- Hartley, B. S. *Philos. Trans. R. Soc. Lond., B* **1970**, *257*, 71-87.
- Alden, R. A.; Wright, C. S.; Kraut, J. *Philos. Trans. R. Soc. Lond., B* **1970**, *257*, 119-124.
- Blow, D. M.; Birktoft, J. J.; Hartley, B. S. *Nature (London)* **1969**, *221*, 337-340.
- MacPhee-Quigley, K.; Vedvick, T. S.; Taylor, P.; Taylor, S. S. *J. Biol. Chem.* **1986**, *261*, 13565-13570.
- MacPhee-Quigley, K.; Taylor, P.; Taylor, S. J. *Biol. Chem.* **1985**, *260*, 12185-12189.

- (67) Schaffer, N. K.; Michel, H. O.; Bridges, A. F. *Biochemistry* 1973, 12, 2946-2950.
- (68) Reddy, M. N.; Maraganore, J. M.; Meredith, S. C.; Heinrikson, R. L.; Kezdy, F. J. *J. Biol. Chem.* 1986, 261, 9678-9683.
- (69) Berman, H. A.; Yguerabide, J.; Taylor, P. *Biochemistry* 1980, 19, 2226-2235.
- (70) Mooser, G.; Sigman, D. S. *Biochemistry* 1974, 13, 2299-2307.
- (71) Taylor, P.; Lappi, S. *Biochemistry* 1975, 14, 1989-1997.
- (72) Berman, H. A.; Taylor, P. *Biochemistry* 1978, 17, 1704-1713.
- (73) Berman, H. A.; Becktel, W.; Taylor, P. *Biochemistry* 1981, 20, 4803-4810.
- (74) Roskoski, R., Jr. *Biochemistry* 1974, 13, 5141-5144.
- (75) Majumdar, R.; Balasubramanian, A. S. *Biochemistry* 1984, 23, 4088-4093.
- (76) Krupka, R. M. *Biochemistry* 1966, 5, 1983-1988.
- (77) Krupka, R. M. *Biochemistry* 1966, 5, 1988-1998.
- (78) Reiner, E.; Aldridge, W. N. *Biochem. J.* 1967, 105, 171-179.
- (79) Hunkapiller, M. W.; Forgac, M. D.; Richards, J. H. *Biochemistry* 1976, 15, 5581-5588.
- (80) Elrod, J. P.; Hogg, J. L.; Quinn, D. M.; Venkatasubban, K. S.; Schowen, R. L. *J. Am. Chem. Soc.* 1980, 102, 3917-3922.
- (81) Stein, R. L.; Elrod, J. P.; Schowen, R. L. *J. Am. Chem. Soc.* 1983, 105, 2446-2452.
- (82) Stein, R. L. *J. Am. Chem. Soc.* 1983, 105, 5111-5116.
- (83) Koehler, K. A.; Hess, G. P. *Biochemistry* 1974, 13, 5345-5350.
- (84) Dafforn, A.; Kerr, P.; Murray, R. R. *Biochim. Biophys. Res. Commun.* 1976, 73, 323-329.
- (85) Wolfenden, R. In *Transition States of Biochemical Processes*; Gandour, R. D.; Schowen, R. L., Eds.; Plenum: New York, 1978; pp 555-578.
- (86) Kettner, C. A.; Shenvi, A. B. *J. Biol. Chem.* 1984, 259, 15106-15114.
- (87) Koehler, K. A.; Lienhard, G. E. *Biochemistry* 1971, 10, 2477-2483.
- (88) Matthews, D. A.; Alden, R. A.; Birktoft, J. J.; Freer, S. T.; Kraut, J. *J. Biol. Chem.* 1975, 250, 7120-7126.
- (89) Brodbeck, U.; Schweikert, K.; Gentinetta, R.; Rottenberg, M. *Biochim. Biophys. Acta* 1979, 567, 357-369.
- (90) Gelb, M. H.; Svaren, J. P.; Abeles, R. H. *Biochemistry* 1985, 24, 1813-1817.
- (91) Dafforn, A.; Neenan, J. P.; Ash, C. E.; Betts, L.; Finke, J. M.; Garman, J. A.; Rao, M.; Walsh, K.; Williams, R. R. *Biochim. Biophys. Res. Commun.* 1982, 104, 597-602.
- (92) Jencks, W. P. *Acc. Chem. Res.* 1976, 9, 425-432.
- (93) O'Brien, R. D. *Biochem. J.* 1969, 113, 713-719.
- (94) Palumaa, P.; Järv, J. *Biochim. Biophys. Acta* 1984, 784, 35-39.
- (95) Tanford, C. *The Hydrophobic Effect*, 2nd ed.; Wiley: New York, 1980; pp 5-20.
- (96) Hasan, F. B.; Elkind, J. L.; Cohen, S. G.; Cohen, J. B. *J. Biol. Chem.* 1981, 256, 7781-7785.
- (97) Dafforn, A.; Jewell, M.; Anderson, M.; Ash, D.; Horvath, D.; Kitson, R.; Margiotta, S.; Rych, G. *Biochim. Biophys. Acta* 1979, 569, 23-30.
- (98) Dafforn, A.; Anderson, M.; Ash, D.; Campagna, J.; Daniel, E.; Horwood, R.; Kerr, P.; Rych, G.; Zappitelli, F. *Biochim. Biophys. Acta* 1977, 484, 375-385.
- (99) Fersht, A. R. *Proc. R. Soc. Lond., B.* 1974, 187, 397-407.
- (100) Berman, H. A.; Decker, M. M. *Biochim. Biophys. Acta* 1986, 872, 125-133.
- (101) Pauling, L. *Am. Sci.* 1948, 36, 51-58.
- (102) Cohen, S. G.; Lieberman, D.; Hasan, F. B.; Cohen, J. B. *J. Biol. Chem.* 1982, 257, 14087-14092.
- (103) Berman, H. A.; Decker, M. M. *J. Biol. Chem.* 1986, 261, 10646-10652.
- (104) Mooser, G.; Schulman, H.; Sigman, D. S. *Biochemistry* 1972, 11, 1595-1602.
- (105) Barnett, P.; Rosenberry, T. L. *J. Biol. Chem.* 1977, 252, 7200-7206.
- (106) Changeux, J. P. *Mol. Pharmacol.* 1966, 2, 369-392.
- (107) Amitai, G.; Ashani, Y.; Gafni, A.; Silman, I. *Biochemistry* 1982, 21, 2060-2069.
- (108) Berman, H. A.; Yguerabide, J.; Taylor, P. *Biochemistry* 1985, 24, 7140-7147.
- (109) Rosenberry, T. L.; Bernhard, S. A. *Biochemistry* 1972, 11, 4308-4321.
- (110) Krupka, R. M. *Biochemistry* 1964, 3, 1749-1754.
- (111) Froede, H. C.; Wilson, I. B.; Kaufman, H. *Arch. Biochem. Biophys.* 1986, 247, 420-423.
- (112) Desire, B.; Saint-Andre, S. *Biochim. Biophys. Acta* 1981, 659, 267-282.
- (113) Shinitzky, M.; Dudai, Y.; Silman, I. *FEBS Lett.* 1973, 30, 125-128.
- (114) Berman, H. A.; Olshefski, D. F.; Gilbert, M.; Decker, M. M. *J. Biol. Chem.* 1985, 260, 3462-3468.
- (115) Page, J. D.; Wilson, I. B. *J. Biol. Chem.* 1985, 260, 1475-1478.
- (116) Wilson, I. B.; Silman, I. *Biochemistry* 1977, 16, 2701-2708.
- (117) Page, J. D.; Wilson, I. B. *Arch. Biochem. Biophys.* 1983, 226, 492-497.
- (118) Froede, H. C.; Wilson, I. B. *Mol. Pharmacol.* 1985, 27, 630-633.
- (119) Schowen, K. B. J. In *Transition States of Biochemical Processes*; Gandour, R. D.; Schowen, R. L., Eds.; Plenum: New York, 1978; pp 225-283.
- (120) Schowen, K. B.; Schowen, R. L. *Methods Enzymol.* 1982, 87, 551-606.
- (121) Venkatasubban, K. S.; Schowen, R. L. *CRC Crit. Rev. Biochem.* 1985, 17, 1-44.
- (122) Jarret, R. M.; Saunders, M. J. *Am. Chem. Soc.* 1985, 107, 2648-2654.
- (123) Belasco, J. G.; Bruice, T. W.; Albery, W. J.; Knowles, J. R. *Biochemistry* 1986, 25, 2558-2564.
- (124) In ref 18 and 20, a transform of eq 25, wherein the weighting factors f_2 and f_3 were expressed in terms of the commitment to proton transfer catalysis (cf. eq 29), was used to fit proton inventories.
- (125) Glasstone, S.; Laidler, K. J.; Eyring, H. *The Theory of Rate Processes*; McGraw-Hill: New York, 1941.
- (126) Kirsch, J. F. In *Isotope Effects on Enzyme-Catalyzed Reactions*; Cleland, W. W., O'Leary, M. H., Northrop, D. B., Eds.; University Park: Baltimore, 1977; pp 100-121.
- (127) Klinman, J. P. *Adv. Enzymol. Relat. Areas Mol. Biol.* 1978, 46, 415-494.
- (128) Hogg, J. L.; Rodgers, J.; Kovach, I.; Schowen, R. L. *J. Am. Chem. Soc.* 1980, 102, 79-85.
- (129) Streitwieser, A., Jr.; Jagow, R. H.; Fahey, R. C.; Suzuki, S. *J. Am. Chem. Soc.* 1958, 80, 2326-2332.
- (130) Kovach, I. M.; Hogg, J. L.; Raben, T.; Halbert, K.; Rodgers, J.; Schowen, R. L. *J. Am. Chem. Soc.* 1980, 102, 1991-1999. The expected effect per D was calculated by taking the β -D effect reported in this reference for the hydration of 1,3-dichloroacetone to the one-fourth power.
- (131) Kovach, I. M.; Quinn, D. M. *J. Am. Chem. Soc.* 1983, 105, 1947-1950.
- (132) Kreevoy, M. M.; Liang, T.-M.; Chang, K.-C. *J. Am. Chem. Soc.* 1977, 99, 5207-5209.
- (133) A normal solvent isotope effect, $D_2O k_E = 1.4$, is also predicted if $k_E^0/k_E^* = 10$, $K_O = 1$ and $\phi^* = 2.1$. However, this case generates a downward-bowing proton inventory. In addition, there is no precedent for a fractionation factor of ~ 2 . Therefore, models in which $\phi^* \gg 1$ are not considered.
- (134) If deacylation were rate limiting for anilides, eq 16 would reduce to $k_{ES} = k_4$ at $pH \gg pK_a$. However, k_4 is the same for acylsilar esters and anilides and, consequently, the larger k_{ES} values for esters require that acylation is rate limiting for anilides.
- (135) Albery, W. J.; Knowles, J. R. *Biochemistry* 1976, 15, 5631-5640.
- (136) The α -D effect for k_{ES} of AChE-catalyzed hydrolysis of PMPF is an unpublished observation of Acheson, S. A. and Quinn, D. M.
- (137) Stackhouse, J.; Nambiar, K. P.; Burbaum, J. L.; Stauffer, D. M.; Benner, S. A. *J. Am. Chem. Soc.* 1985, 107, 2757-2763.
- (138) Jencks, W. P. *Catalysis in Chemistry and Enzymology*; McGraw-Hill: New York, 1969; pp 463-554.
- (139) There may well be more than two chemical transition states in the acylation and deacylation stages of catalysis. This situation would obtain if, for example, proton transfers and heavy atom rearrangements are not concerted.
- (140) Fractional rehybridization was calculated by assuming that the secondary isotope effect depends linearly on the degree of rehybridization of the carbonyl carbon.¹²⁸